INJURY BIOMECHANICS RESEARCH
Proceedings of the Forty First International Workshop

Whole-Body Kinematics in Dynamic Rollover Tests: A Comparison of PMHS Responses for Leading-Side and Trailing-Side Front-Row Seating Positions

David J. Lessley, Patrick Riley, Qi Zhang, Patrick Foltz, Jack Lockerby, Jeremy Seppi, Brian Overby, Mark Sochor, Sara Heltzel, Jeff Crandall, Jason R. Kerrigan

This paper has not been screened for accuracy nor refereed by any body of scientific peers and should not be referenced in the open literature.

ABSTRACT

Rollover crashes present a unique challenge for efforts to improve occupant safety. While these crashes represent less than 3% of all motor vehicle crashes, they are responsible for more than one third of all motor vehicle crash fatalities. Previous studies have utilized anthropometric test devices (ATDs) to study occupant kinematics and injury risk in rollover events, however, the biofidelity of existing ATDs has not yet been demonstrated in the rollover environment due to a notable lack of available benchmarking data specifying the kinematic response of a restrained occupant during a rollover event. The objective of the current study was to characterize the whole-body kinematic response of restrained post mortem human subjects (PMHS) in controlled laboratory rollover tests, in order to generate foundational kinematic response targets to be used in the development and evaluation of ATDs and computational models for use in the study of rollover crashes. Eleven dynamic rollover tests (roll only without ground impact) were conducted using a vehicle test buck that was pitched front-end down by 5 degrees, and was rotated at 360 degrees per second for 360 degrees. The pure roll-only condition simulates the airborne or ballistic phase of a rollover when the vehicle rotates about its center of gravity. Four male PMHS, with anthropometry approximating that of the 50th percentile male, were utilized for these tests. Each PMHS was restrained with a three-point belt restraint and was tested in both leading-side and trailing-side front-row seating positions. Whole-body kinematics were measured using a 26-camera, 500 Hz, 3D motion capture system. PMHS kinematic measurement locations included the head, T1, T4, T10, L1, sacrum, and bilateral acromia. Occupant displacement relative to the vehicle buck was quantified for all measurement locations for the X-axis (fore-and-aft), Y-axis (lateral), and Z-axis (vertical) directions. Additionally the spine was divided into five segments (head to T1, T1 to T4, T4 to T10, T10 to L1, and L1

to Sacrum) to describe the intrasegmental kinematics of the spine, including segment rotations as well as spinal extension and compression. The utilized vehicle test buck was designed to mimic a contemporary mid-sized SUV in the US market, but incorporated simplified rigid seats and interior components to improve test-to-test repeatability and also visualization of the occupant kinematic measurement locations with the optically-based 3D motion capture system. The kinematic results generally demonstrated highly characteristic responses observed across all four tested PMHS. Regardless of seating position, the head and spine measurement locations generally moved outboard and upward during the event, with locations superior to T10 also moving rearward. Displacement of the unloaded shoulder was observed to be very similar across the two seating positions, however, in contrast, the displacement of the loaded shoulder was quite different from leading-side to trailing-side seating position. The greatest vertical (upward) displacements were consistently observed for the leading-side seating position. The spine was generally found to elongate during the tests, with the greatest extensions occurring in the cervical and lumbar segments, while the T10 to L1 segment consistently experienced compression. Spinal extensions were generally insensitive to seating position. Regardless of seating position, spine segments superior to T10 predominately rotated rearward, while those inferior to T10 predominately rotated forward. The reported data represent the most complete set of kinematic response targets for a restrained occupant in a dynamic rollover condition, and are immediately useful for efforts to evaluate and improve existing ATDs and computational models for use in the rollover crash environment.

INTRODUCTION

Rollover crashes are a serious public health problem in the United States. While crashes that involve a vehicle rollover account for less than three percent of total crashes, they account for more than one third of all vehicle occupant fatalities (NHTSA 2010). Such statistics highlight the inherent potential for occupant injury that is associated with rollover type crashes.

Mitigating rollover-related injuries presents a unique challenge for efforts to improve occupant safety, which has motivated rollover research since the late 1950s. Early rollover research began with Shoemaker (1959), who used lap belt-restrained dummies in vehicle simulators to document occupant motions during vehicle rotations on a spit-type platform (Bahling et al., 1990). Shoemaker (1959) noted that the dummies were able to make head contact with the roof in these early tests, despite the use of a lap belt. Rollover studies that soon followed, attempted to understand the effect of restraint use on injury outcome (Campbell, 1962; Hight et al., 1972; Stone, 1974; Huelke, et al., 1977a; Heulke et al., 1977b; Evans, 1988). Other research efforts specifically investigated how roof crush affected the injury outcome of belted occupants (Huelke et al., 1972; Huelke et al., 1973; Anderson, 1974; Bahling et al., 1990). Finally, more recent studies began to recognize the importance of, and focused on, occupant kinematics during the rollover event (Herbst et al., 1996; Moffatt et al., 1997; Pywell et al., 1997; Moffatt et al., 2003).

Rollover occupant injuries have been widely hypothesized to be highly sensitive to occupant position and orientation at the instance of occupant contact with the vehicle interior, regardless of the mechanism of impact. Thus, understanding occupant kinematics throughout rollover crashes is critical to countermeasure development and occupant protection strategies. Despite its importance, the study of occupant kinematics in the dynamic rollover environment has remained limited. A number of studies have utilized inverted vertical hang tests to study occupant head excursion statically (Bahling et al., 1990; Arndt et al., 1995; Herbst et al., 1996; James et al., 1997; Moffatt et al., 1997; Ward et al., 2001; Moffatt et al., 2003). However, studies quantifying the dynamic excursion of restrained occupants during rollovers are very sparse with the exception of those performed by Moffatt et al. (1997), Pywell et al. (1997), and Moffatt et al. (2003), but even these have been limited primarily to the study of peak head excursions.

Additionally, much of the previous study of occupant response in rollovers has traditionally been carried out with the Hybrid III anthropomorphic testing device (ATD). The Hybrid III, however, has been shown to respond differently (exhibiting less excursion) in rollover conditions than volunteer or cadaver subjects, particularly in terms of lateral excursion (Moffatt et al., 1997; Moffatt et al., 2003). It has been reasonably hypothesized that these differences arise from the greater spine stiffness in the Hybrid III, which was designed for frontal impact response rather than for the lower loads associated with the pre-impact rollover environment (Moffatt et al., 1997; Moffatt et al., 2003). While the existing body of rollover research is undoubtedly both broad and valuable, the absence of

research that comprehensively characterizes the whole-body kinematic response of a restrained occupant in the dynamic rollover environment has led to a notable lack of benchmarking data for the evaluation and development of ATDs. Thus, the biofidelity of existing ATDs has not yet been demonstrated in the rollover environment.

In order to establish appropriate kinematic response targets to evaluate and guide ATD performance for use in the study of rollovers, additional human response data is needed for a restrained occupant in the rollover environment. However, effectively measuring such occupant responses in the complex rollover environment has been historically difficult. Recently, however, technological advances have enabled detailed whole-body kinematics to be obtained using 3D motion capture technology under high-rate, dynamic impact conditions (Lessley et al., 2011), thus, making it possible to quantify detailed occupant motions that were largely impossible to quantify even a decade ago.

The current study is part of a larger multi-step research effort that aims to 1) characterize whole-body kinematic response of post mortem human subjects (PMHS) in a variety of rollover conditions and 2) to evaluate the biofidelity of existing ATDs in identical rollover conditions. More specifically, the objective of the current study is to characterize the whole-body kinematic response of restrained PMHS in controlled laboratory rollover tests, in order to generate foundational kinematic response targets to be used in the development and evaluation of ATDs and computational models for use in the study of rollover crashes.

METHODS

Test Setup and Fixture

Eleven dynamic rollover tests (roll only without ground impact) (Table 1) were conducted with four adult male PMHS using a dynamic rollover test system (DRoTS). The test methodology utilized for the reported tests was described previously in detail by Zhang et al. (2013), however, a summary of the test methodology relevant to the presented results is included here. The DRoTS test fixture was designed to perform controlled and repeatable rollover crash tests in the laboratory with actual full-sized vehicles (Kerrigan et al., 2011) (Figure 1). For these reported tests, however, only the rotational aspect of the DRoTS was utilized to rotate a customized test buck around its center of gravity (cg) without ground contact. Figure 1 illustrates the DRoTS and the roll rate and roll angle achieved as a function of time during the presented tests. During each test, the vehicle buck was accelerated to a peak angular rate of 360 degrees per second over the roll interval from 0 to 125 degrees. From 125 degrees to approximately 290 degrees the roll rate remained nearly constant. The vehicle buck was then decelerated to a stop over the roll interval from approximately 290 to 360 degrees. Both the acceleration and deceleration phases of the rollover event were nearly linear. The test buck (Figure 2) was designed to approximate a vehicle-based restraint environment with simplified boundary conditions which allowed for separation of parameters, increased lines of sight for measuring occupant motion, and ease of test reproducibility. The exterior and interior geometry of the buck represented an average of twelve contemporary full-sized crossover vehicles in the US, while restraint, toe pan, and seat locations matched one of the 12 vehicles (Foltz et al., 2011; Zhang et al.,2013).

Table 1. Test Matrix.

Occupant Position	Roll Rate (deg/sec)	Total Roll Angle (deg)	Belt Pretension (N)	Subject #580	Subject #570	Subject #571	Subject #609
Leading-Side	360	360	30	1890	1897, 1898	1905, 1906	1913, 1914
Trailing-side	360	360	30	1894	1902	1910	1918

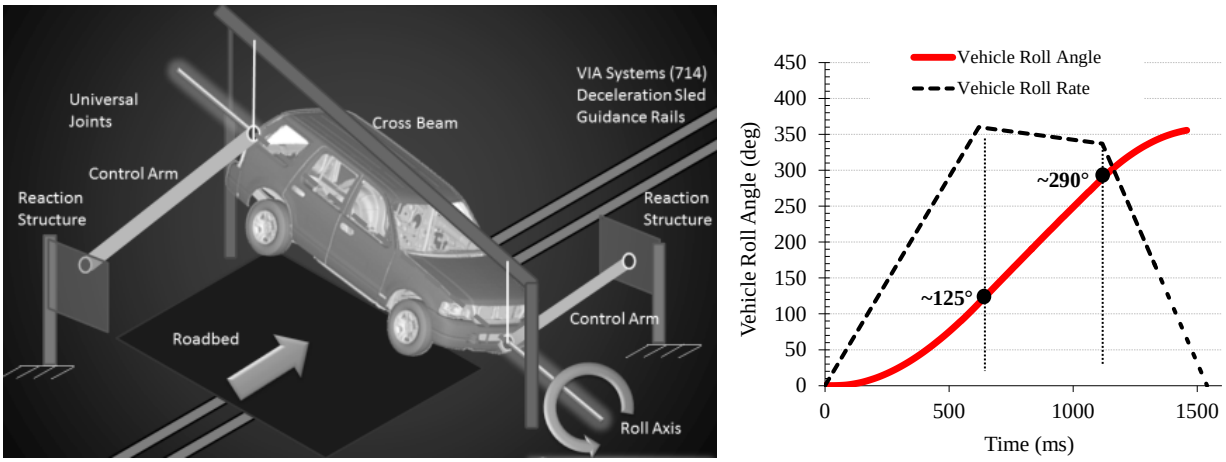

Figure 1. Dynamic rollover test system (DRoTS) and dynamic rotation characteristics used for the current study.

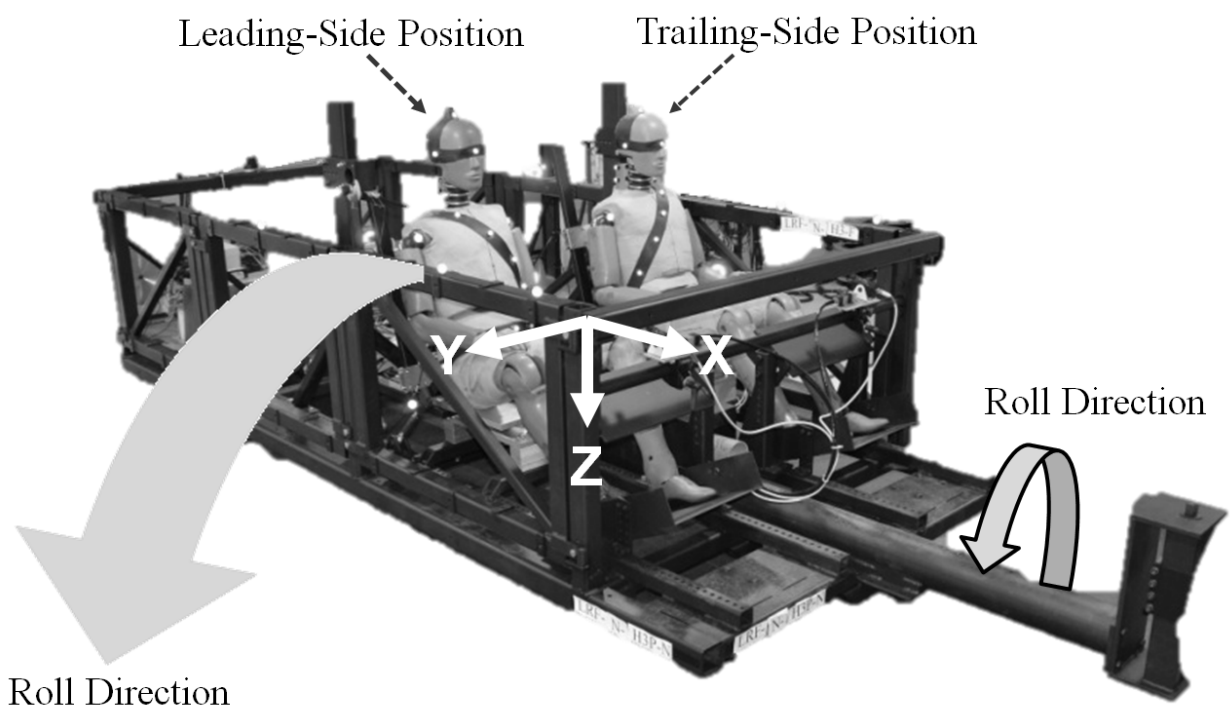

Figure 2. Parametric buck, seating positions, roll direction, and SAE vehicle coordinate system. Illustrated with 50th percentile Hybrid III ATDs occupying both seats.

Using the DRoTS, the buck was pitched front-end down by 5 degrees, and was rotated at 360 degrees per second for 360 degrees to study occupant kinematics during the rollover event. The pure roll-only condition simulates the airborne or ballistic phase of a rollover when the vehicle rotates about its center of gravity (Moffatt et al., 1997; Moffatt et al., 2003; Zhang et al., 2013). The start of each test was indicated by an electrical trigger event that occurred simultaneously with the roll initiation. The test start time is denoted by, t_0.

Each PMHS was tested in both leading-side and trailing-side front-row seating positions (Table 1). Only one PMHS occupied the buck during any given test. A water ballast dummy (Figure 3), with mass equal to a 50th percentile male, was secured in the unoccupied seat to maintain consistent mass distribution and inertial properties of the buck. Each PMHS was restrained with a fixed-length three-point belt restraint without retractor (Zhang et al., 2013). The D-ring, buckle, and latch plate (Takata, Inc.) were standard vehicle parts from a model year 2012 truck, and the utilized webbing was characterized previously by Shaw et al. (2009) (Industries, International twill pattern

13195, 6.8% elongation, 26.7 kN minimum tensile strength). The belt webbing was anchored to the vehicle at the outboard lap belt attachment and at the base of the B-pillar with turnbuckles that facilitated manual belt pretensioning prior to the test (Zhang et al., 2013). The belt webbing was manually pretensioned to 30 N prior to each of the eleven reported tests. Figure 3 provides a pretest illustration of the secured water ballast dummy, the seated PMHS, and restraint configuration.

Subject Details and Procedure

Four adult male PMHS, with anthropometry approximating that of the 50th percentile male, were utilized for the reported tests (Table 2). A total of 36 tests were performed, however, this study focuses only on the eleven pure roll tests with the PMHS seated in either the leading-side or trailing-side seating positions. The subjects were acquired and prepared with the approval of and in accordance with the policies and procedures of the UVA Center for Applied Biomechanics Oversight Committee. The subjects were preserved by freezing and confirmed free of infectious diseases including HIV and Hepatitis B and C.

Table 2. PMHS Characteristics.

PMHS ID	580	570	571	609
Gender	Male	Male	Male	Male
Age at Time of Death	51	59	58	58
Cause of Death	Lung Cancer	Heat Stroke	Cardiac Arrest	Malignant Brain Neoplasm
Body Mass (kg)	68.9	83	83.4	86.2
Stature (cm)	191	175	175	180

Prior to the testing the subjects were wrapped with a single layer of Coban™ (3M™) self-adhering wrap to limit the spread of biological fluids, to strain-relieve and protect instrumentation wires, and to serve as a marking surface. This technique has been utilized in a number of previous studies with PMHS (Shaw et al., 2009; Lessley et al., 2010; Lopez-Valdes et al.,2010; Forman et al. 2013). Prior to each test, the subject was positioned in a manner that closely approximately the UMTRI standard driving position (Schneider et al., 1983) which has been commonly targeted in previous frontal and side impact testing (Shaw et al., 2009; Lessley et al., 2010), and was described in detail by Zhang et al. (2013). The PMHS midline was aligned with the seat centerline with the posterior aspect of the torso in contact with rigid seatback and feet in contact with the toe pan (Figure 3). Torso, femur, tibia, sternum, and head angles were measured and held consistent across tests for a given PMHS. Additionally, seated anthropometry was measured and recorded for each PMHS. The hands were secured to the superior aspect of the thigh in a natural resting position to prevent the upper extremities from obscuring motion tracking targets during the rollover event. The head was secured using 25.4 mm wide 3M™ painters' tape (Figure 3). This tape was cut approximately midway through its width to create a stress concentration that allowed the tape to tear away at the initiation of the test. With the subject positioned, spherical motion tracking markers were secured to all selected kinematic measurement locations immediately prior to the first test. Finally, the subject's lungs were inflated with 2.5 liters of air, delivered through a tracheal tube which was left open to the atmosphere following the single inflation cycle. Figure 3 illustrates the pretest subject position for the leading-side seating position (far-side seating position similar). To assess PMHS response repeatability, a single repeated test in the leading-side seating position was performed for subjects 2, 3, and 4 (Table 1).

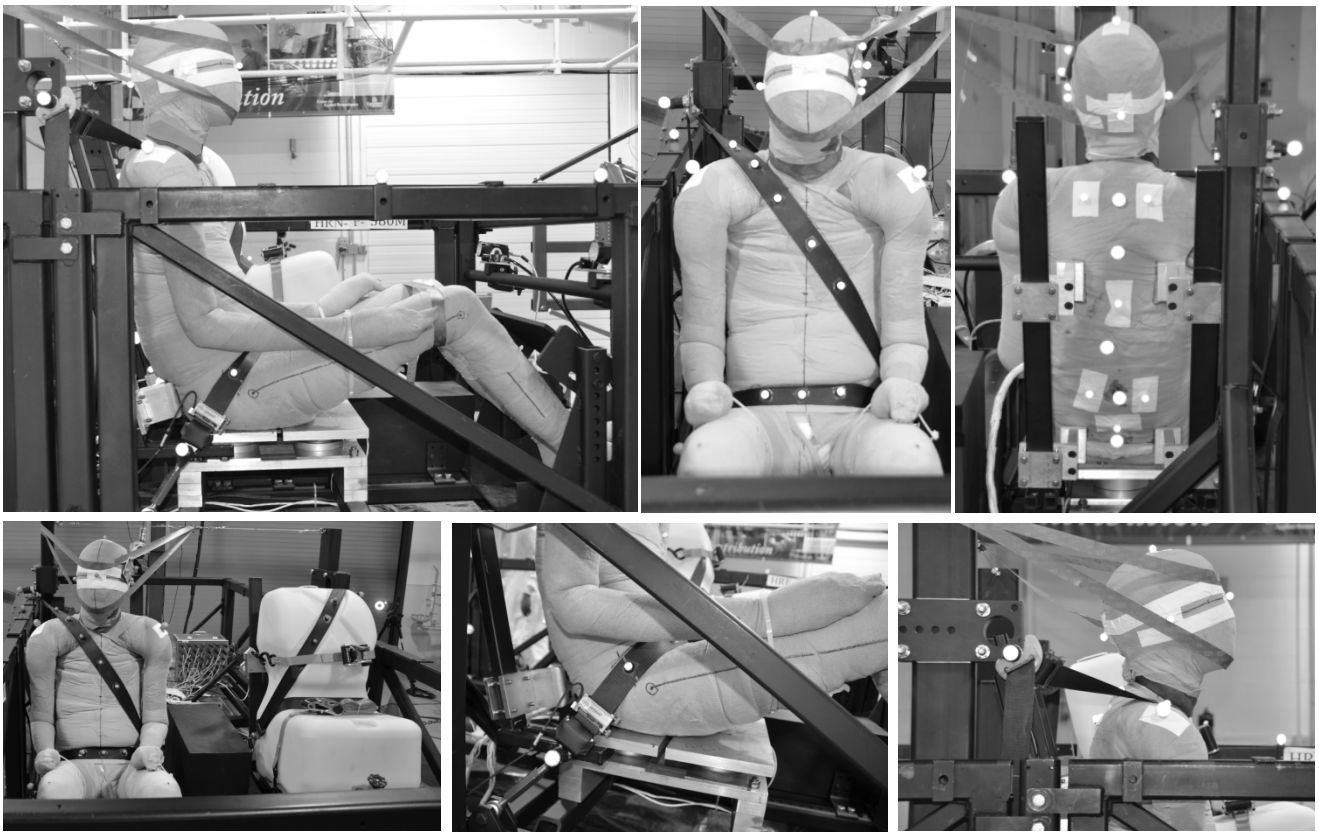

Figure 3. Pretest subject position and restraint configuration for the leading-side seating position (far-side seating position similar).

Measurement of Occupant Kinematics

PMHS and buck kinematics data were captured at 500 Hz with a 26 camera optoelectronic stereophotogrammetric system (OSS) (Vicon MX, Vicon, Los Angeles, CA) (Figure 4). The motion capture system tracked the trajectories of spherical retroreflective markers through a calibrated 3D space within the cameras' collective field of view. Markers were secured to the head, spine, and shoulders of each PMHS. Additional markers were attached to the restraints and rigid structure of the vehicle buck (Figure 4). Using a methodology reported in detail by Lessley et al. (2011), rigid body mechanics were applied to determine ATD kinematics with respect to the local vehicle coordinate system using coordinate transformation. Figure 5 depicts two coordinate systems related by a time varying transformation matrix (Equation 1). The position of a given point, P, relative to a global coordinate system (coordinate system #2 in Figure 5) can be determined relative to a local coordinate system (coordinate system #1 in Figure 5) using Equation 1. The 3D displacement relative to the local (i.e. vehicle) coordinate system is determined by the change in position of point, P, with time using Equations 2 – 4.

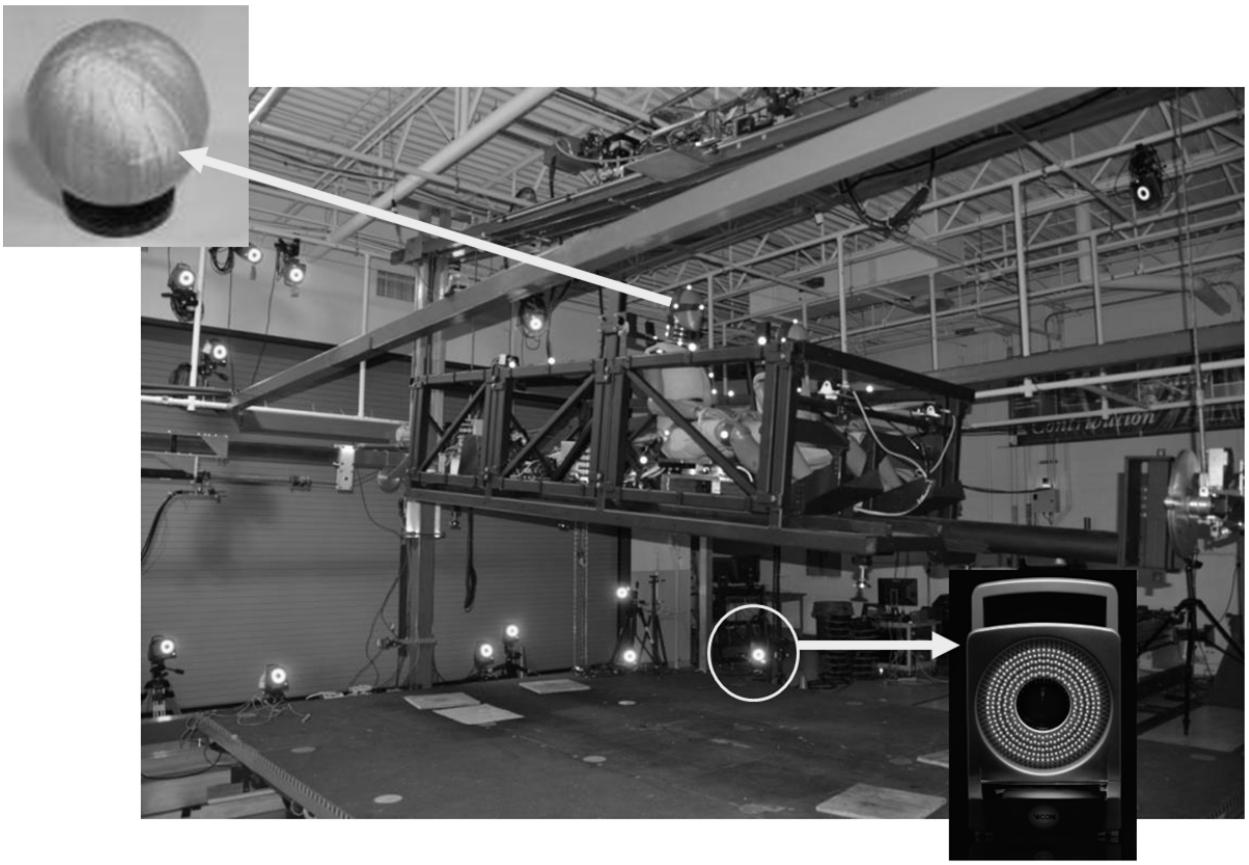

Figure 4. DRoTS system combined with a 3D motion capture system. Illustrated with Hybrid III ATDs occupying both seating positions.

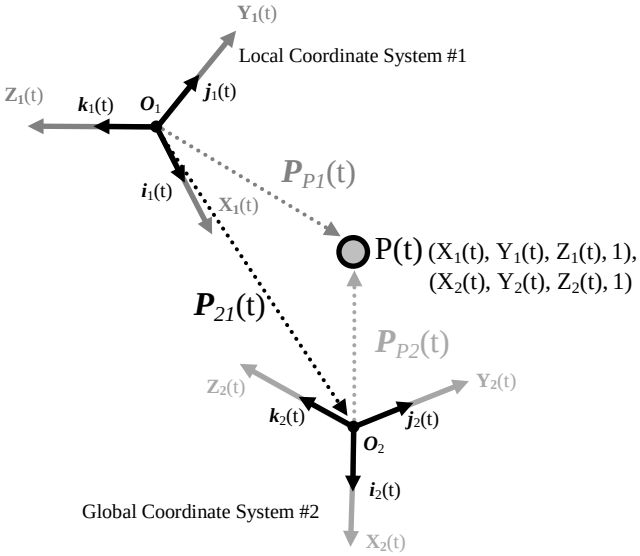

Figure 5. Relationship between local and global 3D coordinates of a given point P.

$$\begin{bmatrix} X_1(t) \\ Y_1(t) \\ Z_1(t) \\ 1 \end{bmatrix} = \begin{bmatrix} (\vec{i}_2(t) \circ \vec{i}_1(t)) & (\vec{j}_2(t) \circ \vec{i}_1(t)) & (\vec{k}_2(t) \circ \vec{i}_1(t)) & (\vec{P}_{21}(t) \circ \vec{i}_1(t)) \\ (\vec{i}_2(t) \circ \vec{j}_1(t)) & (\vec{j}_2(t) \circ \vec{j}_1(t)) & (\vec{k}_2(t) \circ \vec{j}_1(t)) & (\vec{P}_{21}(t) \circ \vec{j}_1(t)) \\ (\vec{i}_2(t) \circ \vec{k}_1(t)) & (\vec{j}_2(t) \circ \vec{k}_1(t)) & (\vec{k}_2(t) \circ \vec{k}_1(t)) & (\vec{P}_{21}(t) \circ \vec{k}_1(t)) \\ 0 & 0 & 0 & 1 \end{bmatrix} * \begin{bmatrix} X_2(t) \\ Y_2(t) \\ Z_2(t) \\ 1 \end{bmatrix} \quad [1]$$

$$\Delta X_1(t) = X_1(t) - X_1(t_0) \quad [2]$$

$$\Delta Y_1(t) = Y_1(t) - Y_1(t_0) \quad [3]$$

$$\Delta Z_1(t) = Z_1(t) - Z_1(t_0) \quad [4]$$

Figure 6 illustrates the anatomical measurement locations on all tested PMHS which included the head cg, T1 (spinous process), T4 (spinous process), T10 (spinous process), L1 (spinous process), sacrum, left acromion (LAc) and right acromion (RAc). The spinal markers (T1-sacrum) were secured to anchors that were surgically implanted into the selected spinous processes and sacrum of each PMHS. The shoulder markers (LAc and RAc) were secured to the external surface of the skin on the superior aspect of the acromion. Multiple markers secured to the head provided the kinematics of the head CG.

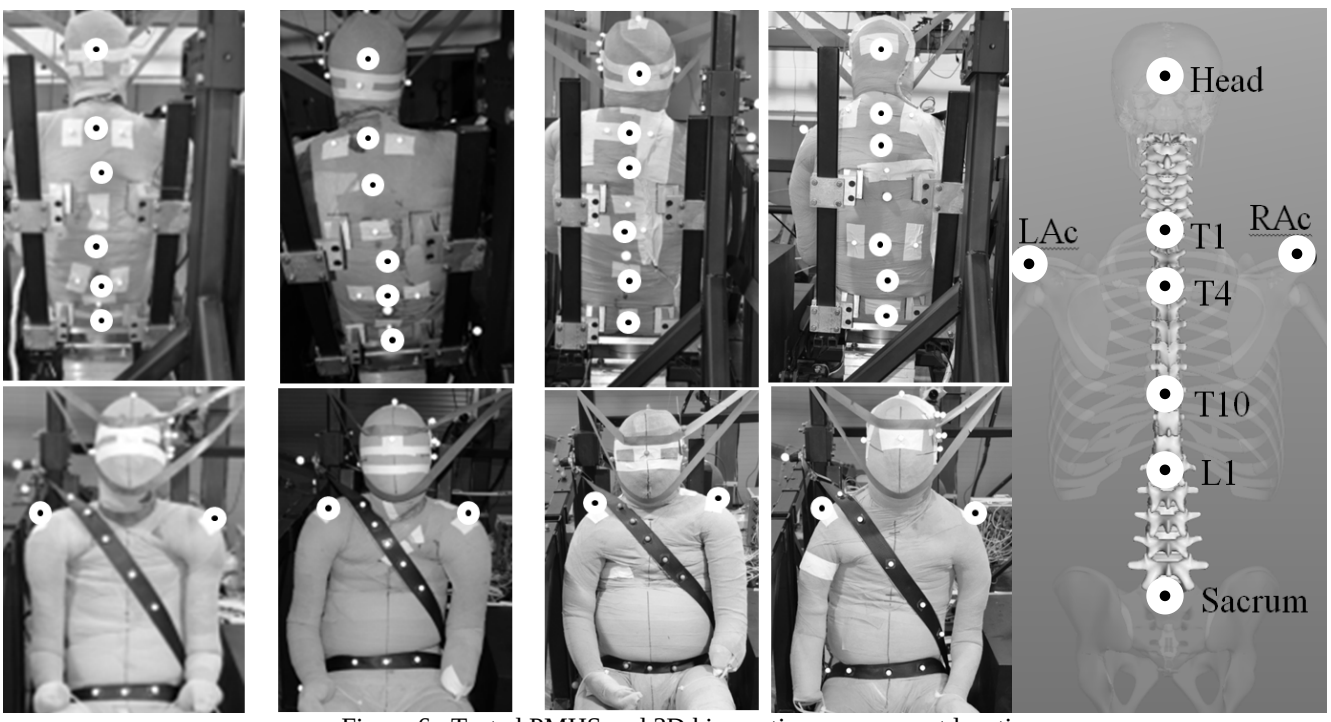

Figure 6. Tested PMHS and 3D kinematic measurement locations.

Additional Instrumentation

While the focus of the current study was on occupant kinematics obtained from the 3D motion capture system, additional instrumentation was also employed for the tests. This data, however, is beyond the scope of the current study and is not specifically presented here. The additional instrumentation included belt tension gages located on the upper shoulder belt, outer lap belt, and inboard lap belt. A 6 degree-of-freedom accelerometer and angular rate sensor package was mounted to the head while tri-axial accelerometer packages were mounted to the T8 vertebra and sacrum. The rigid seat pan was divided into two equally sized rectangular aluminum plates that nearly joined to create a continuous surface (Figure 3). Each seat pan plate was supported by a pair of multi-axis load cells mounted to the lower frame of the vehicle buck. Multiple on-board and off-board high speed (500 Hz) video cameras (HR-CAM,GX-5, NAC Image Technology, Simi Valley, CA) were used to record and visualize the tests.

Kinematic Data Processing and Presentation

Occupant displacement relative to the vehicle buck was quantified for all measurement locations for the X-axis (forward), Y-axis (laterally to occupant's right), and Z-axis (downward) directions (Figure 7). The described displacement directions are in accordance with those specified by SAE J1733 (SAE, 1994). The occupant's spine was divided into five segments (head to T1, T1 to T4, T4 to T10, T10 to L1, and L1 to Sacrum) to describe additional kinematics of the spine, including segment rotations as well as spinal extension and compression (Figure 8). For a given spine segment let the superior location be referred to as "SL" and the inferior location be referred to as "IL". For a given spine segment, ***i***, the extension, X-axis rotation, and Y-axis rotation are provided by Equations 5-12 and are illustrated in Figure 8. Segment extension is the positive change in distance between the corresponding segment endpoints (SL and IL). Positive Y-axis rotation is rearward rotation of the segment (i.e. SL moves backward (negative X-axis displacement relative to IL)). Positive X-axis rotation is rotation of the segment to the right when reviewed from behind (i.e. SL moves right (positive Y-axis displacement) relative to IL). While each kinematic response parameter was measured with time during each rollover test, the PMHS response for each parameter, β_j, is plotted as a function of vehicle roll angle, θ, which is a more intuitive method for presenting the kinematic data.

Kinematic Response Corridors

In order to produce kinematic biofidelity targets (i.e. response corridors) it was necessary to quantify the responses of multiple test subjects for a given kinematic parameter, β_j. This was accomplished by calculating a mean PMHS response value, $\overline{\beta_j}$, at each time, *t*, during the test event from the number, N, of available individual response values (Equation 13). To quantify the response variation across individual tests for a given response parameter, the standard deviation, $SD_{\beta_j}(t)$, for each parameter of interest, $\beta_j(t)$, was calculated using Equation 14 from the number, N, of available individual responses. Plotting the values of $\overline{\beta_j}(t) \pm SD_{\beta_j}(t)$ for the entire rollover event produced a one standard deviation (1 SD) corridor around the average PMHS response for a given kinematic response parameter as a function of time. In order to present the kinematic data most intuitively, the kinematic response corridors are presented instead as a function of vehicle roll angle, θ. Thus, a given PMHS response is given by $\beta_j(\theta)$, and the associated response corridors are given by $\overline{\beta_j}(\theta) \pm SD_{\beta_j}(\theta)$.

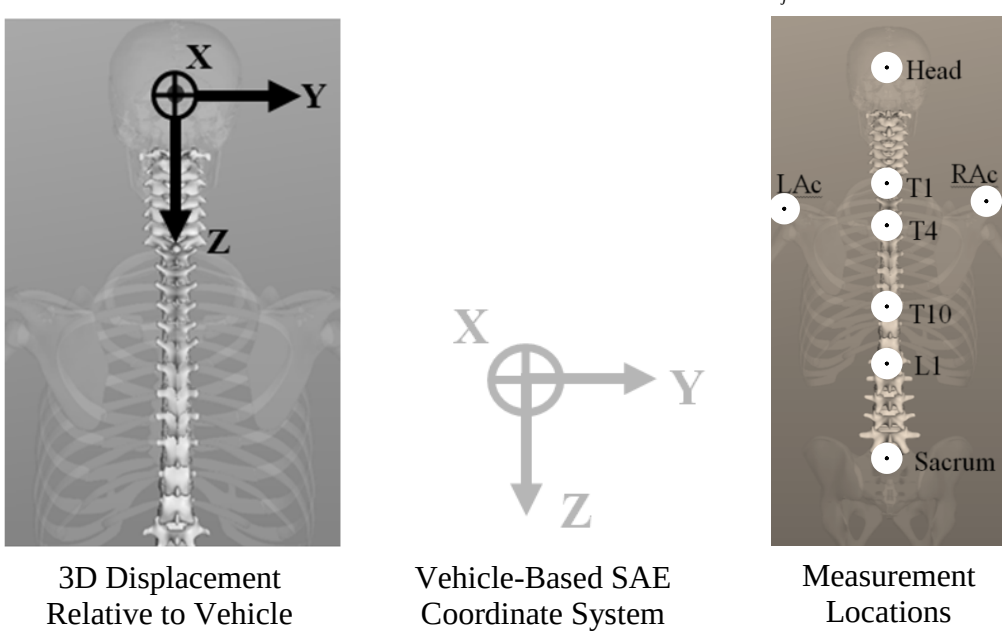

Figure 7. 3D anatomical displacements measured with respect to the vehicle buck.

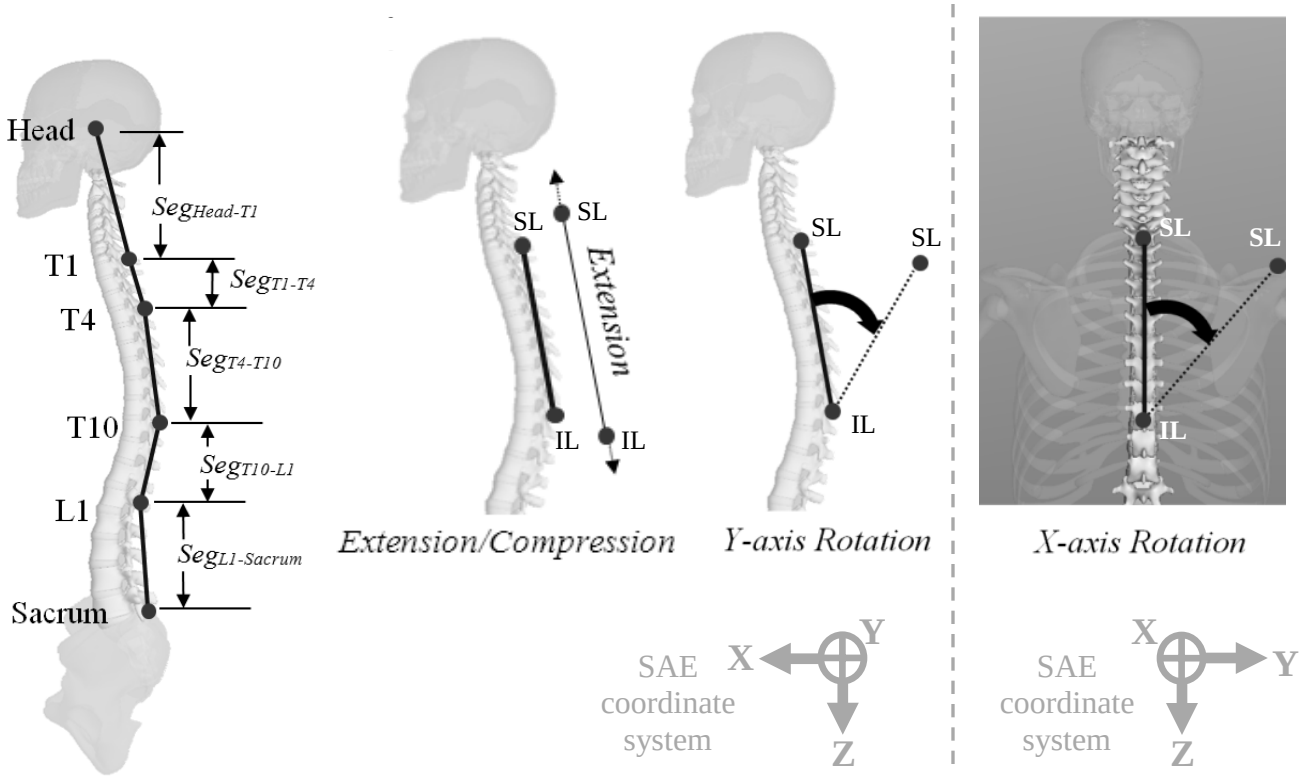

Figure 8. Extension, compression, and rotation of the five spine segments.

$$Seg_{i_{Length}}(t) = \sqrt{[SL_{i_X}(t) - IL_{i_X}(t)]^2 + [SL_{i_Y}(t) - IL_{i_Y}(t)]^2 + [SL_{i_Z}(t) - IL_{i_Z}(t)]^2} \quad [5]$$

$$Seg_{i_{Extension}}(t) = Seg_{i_{Length}}(t) - Seg_{i_{Length}}(t_0) \quad [6]$$

$$\Delta Seg_{i_X}(t) = SL_{i_X}(t) - IL_{i_X}(t) \quad [7]$$

$$\Delta Seg_{i_Y}(t) = SL_{i_Y}(t) - IL_{i_Y}(t) \quad [8]$$

$$Seg_{i_{X-axis\ Angle}}(t) = \arcsin\left[\frac{\Delta Seg_{i_Y}(t)}{Seg_{i_{Length}}(t)}\right] * \frac{180}{\pi} \quad [9]$$

$$Seg_{i_{Y-axis\ angle}}(t) = -\arcsin\left[\frac{\Delta Seg_{i_X}(t)}{Seg_{i_{Length}}(t)}\right] * \frac{180}{\pi} \quad [10]$$

$$Seg_{i_{X-axis\ Rotation}}(t) = Seg_{i_{X-axis\ Angle}}(t) - Seg_{i_{X-axis\ Angle}}(t_0) \quad [11]$$

$$Seg_{i_{Y-axis\ Rotation}}(t) = Seg_{i_{Y-axis\ Angle}}(t) - Seg_{i_{Y-axis\ Angle}}(t_0) \quad [12]$$

$$\overline{\beta_j}(t) = \frac{1}{\mathrm{N}} \sum_{\mathrm{k}=1}^{\mathrm{N}} \beta_{j_k}(t) \quad [13]$$

$$\mathrm{SD}_{\beta_j}(t) = \sqrt{\frac{1}{\mathrm{N}} \sum_{\mathrm{k}=1}^{\mathrm{N}} (\beta_{j_k}(\mathrm{t}) - \overline{\beta_j}(\mathrm{t}))^2} \quad [14]$$

RESULTS

Eleven dynamic, pure rollover tests (without ground contact) were successfully conducted with four adult male PMHS. The achieved roll angle time-history curves for all eleven conducted tests are provided in Figure 9. Each test lasted for approximately 1.5 seconds and the DRoTS produced a very consistent and repeatable input roll-angle time history across all eleven PMHS tests. Each of Figures 10 and 11 provides an overall view of the rollover test with the PMHS seated in either the leading-side or trailing-side seating position. More specifically, Figures 10 and 11 use selected still-frame images taken from an off-board high-speed video camera to illustrate the occupant and vehicle motions at 45 degree intervals from 0 to 360 degrees. For the leading-side position (Figure 10) the PMHS was initially displaced inboard during the first 90 degrees of rotation and was then displaced outboard throughout the remainder of the rollover event. For the trailing-side position (Figure 11) the PMHS was displaced outboard for nearly the entire rollover event, with the exception of the head and upper spine which were displaced slightly inboard at the end of the tests during following the rotational deceleration of the vehicle buck.

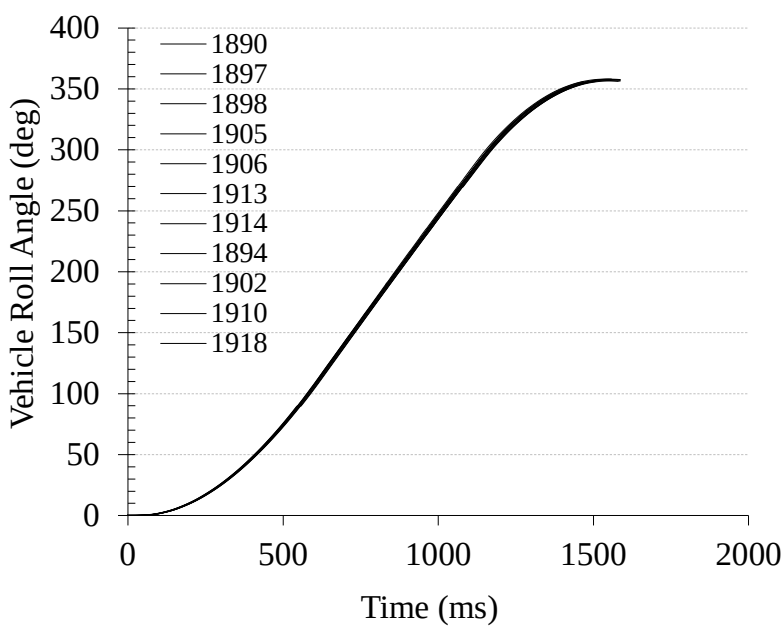

Figure 9. Vehicle roll-angle time-history curves for all presented PMHS tests.

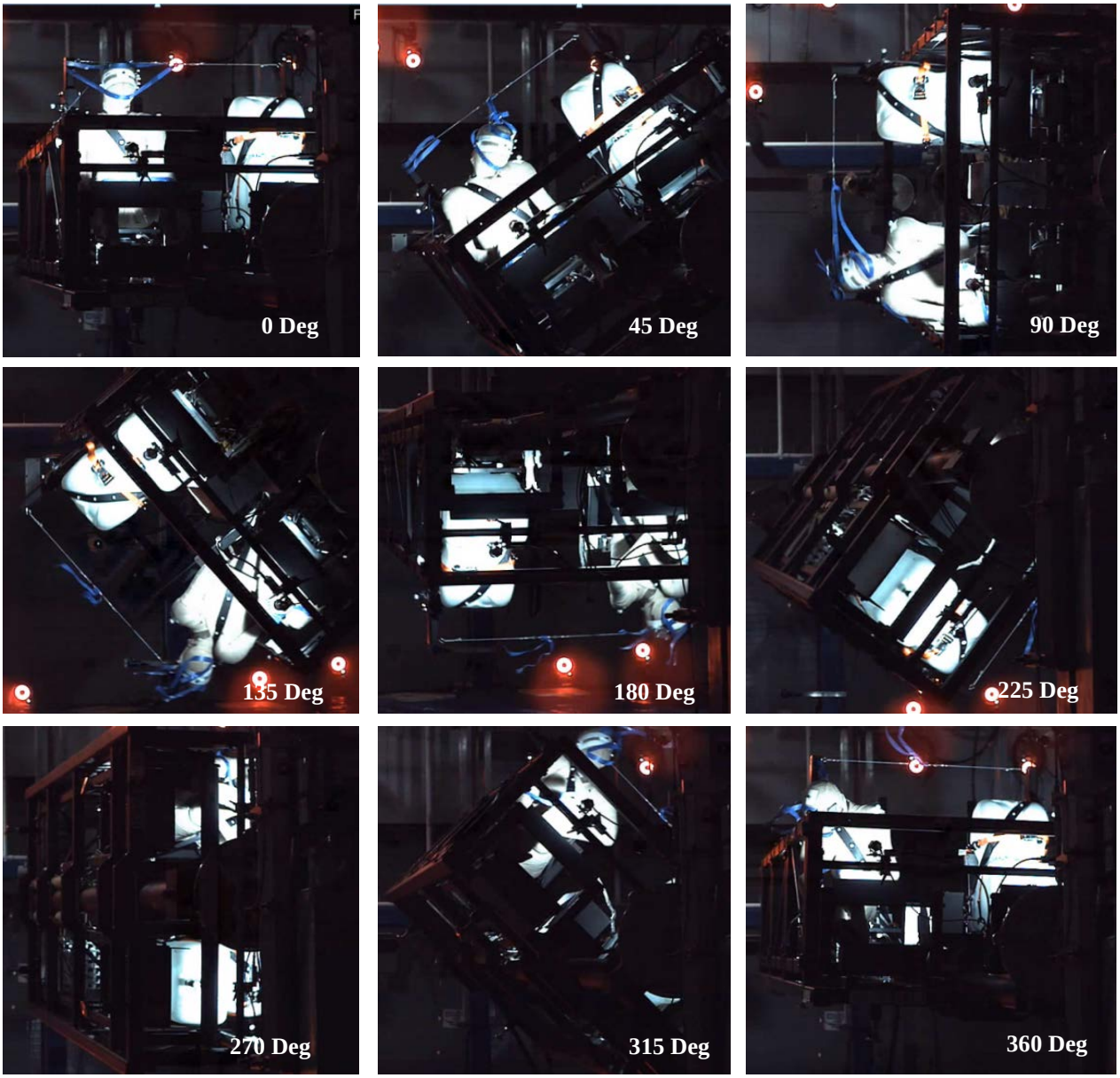

Figure 10. Dynamic rollover test with the occupant in the leading-side seating position. Subject 580 illustrated, other subjects similar.

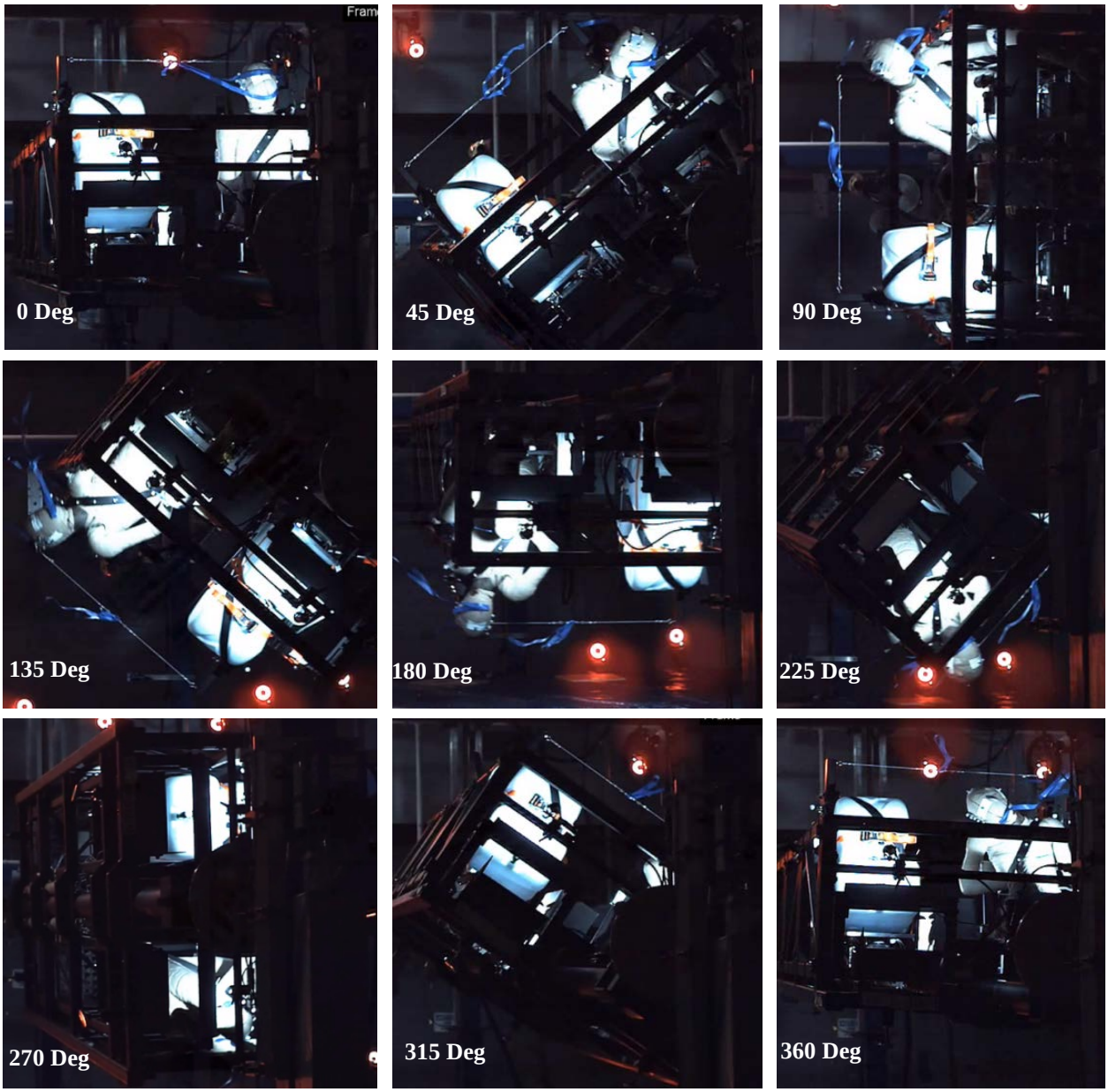

Figure 11. Dynamic rollover tests with the occupant in the trailing-side seating position. Subject 580 illustrated, other subjects similar.

PMHS Kinematic Response

Kinematic data was successfully collected throughout each test producing kinematic corridors for each kinematic parameter described above. Figure 12 provides selected occupant kinematic responses as a function of vehicle roll angle, and illustrates the resulting 1 SD kinematic corridors constructed from multiple measured responses. Figures 13 and 14 provide a comparison of response corridors for occupant displacement with respect to the vehicle for both leading-side and trailing-side seating positions. Mean peak occupant displacements in the X-,Y-, and Z-axis directions for both seating positions are illustrated in Figure 15. Mean peak spine segment extensions and rotations are provided in Figures 16 and 17. A comparison of kinematic corridors for spine segment extensions and rotations are provided in Appendix A. Additionally, Appendix A provides a summary of peak values for all measured parameters in all conducted tests in Tables A1 and A2.

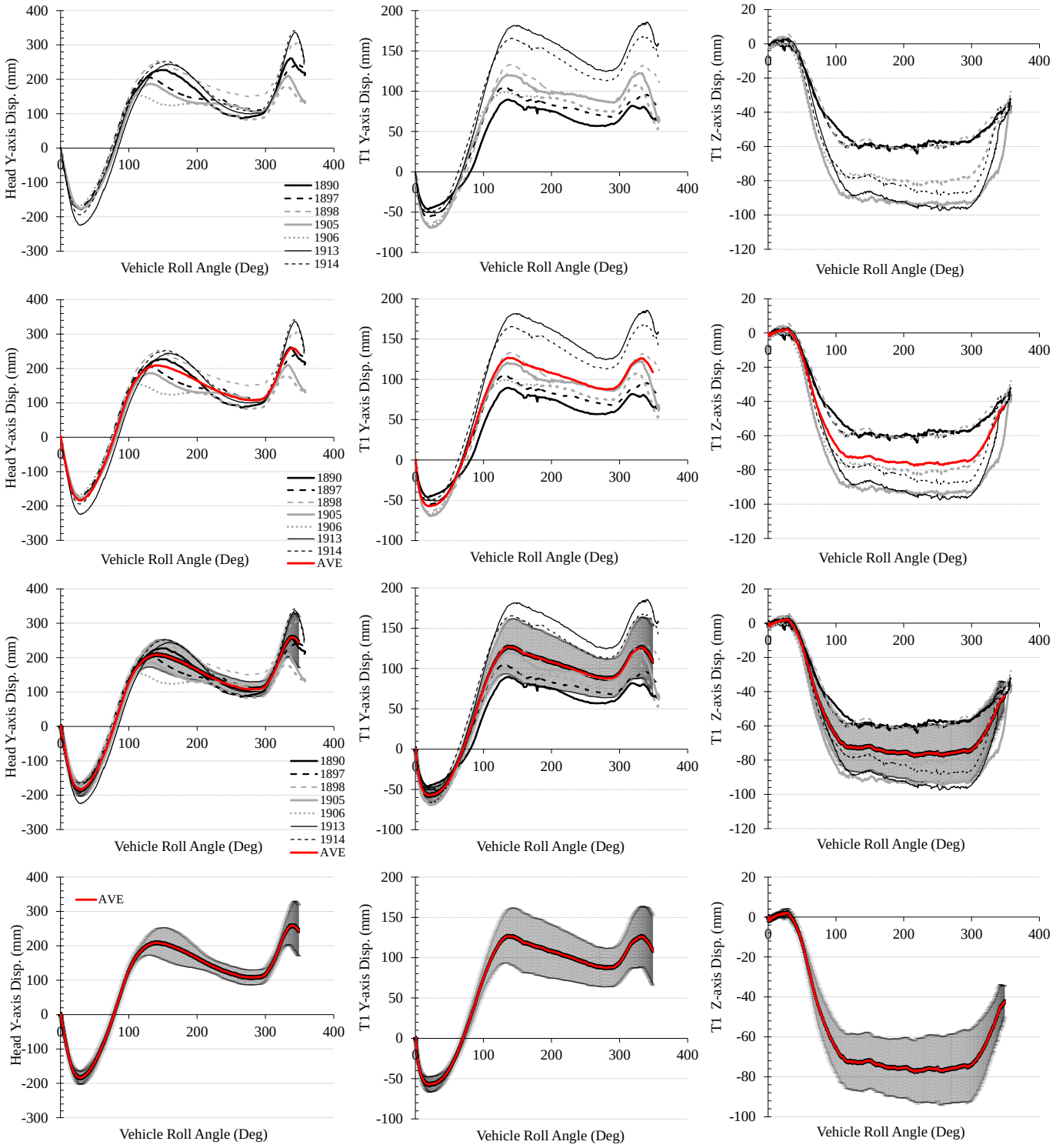

Figure 12. Example kinematic parameters as a function of vehicle roll angle. Individual responses (1st row); individual responses with PMHS average (2nd row); individual responses with PMHS average and 1 SD corridor (3rd row); and PMHS average and 1 SD corridor only (4th row).

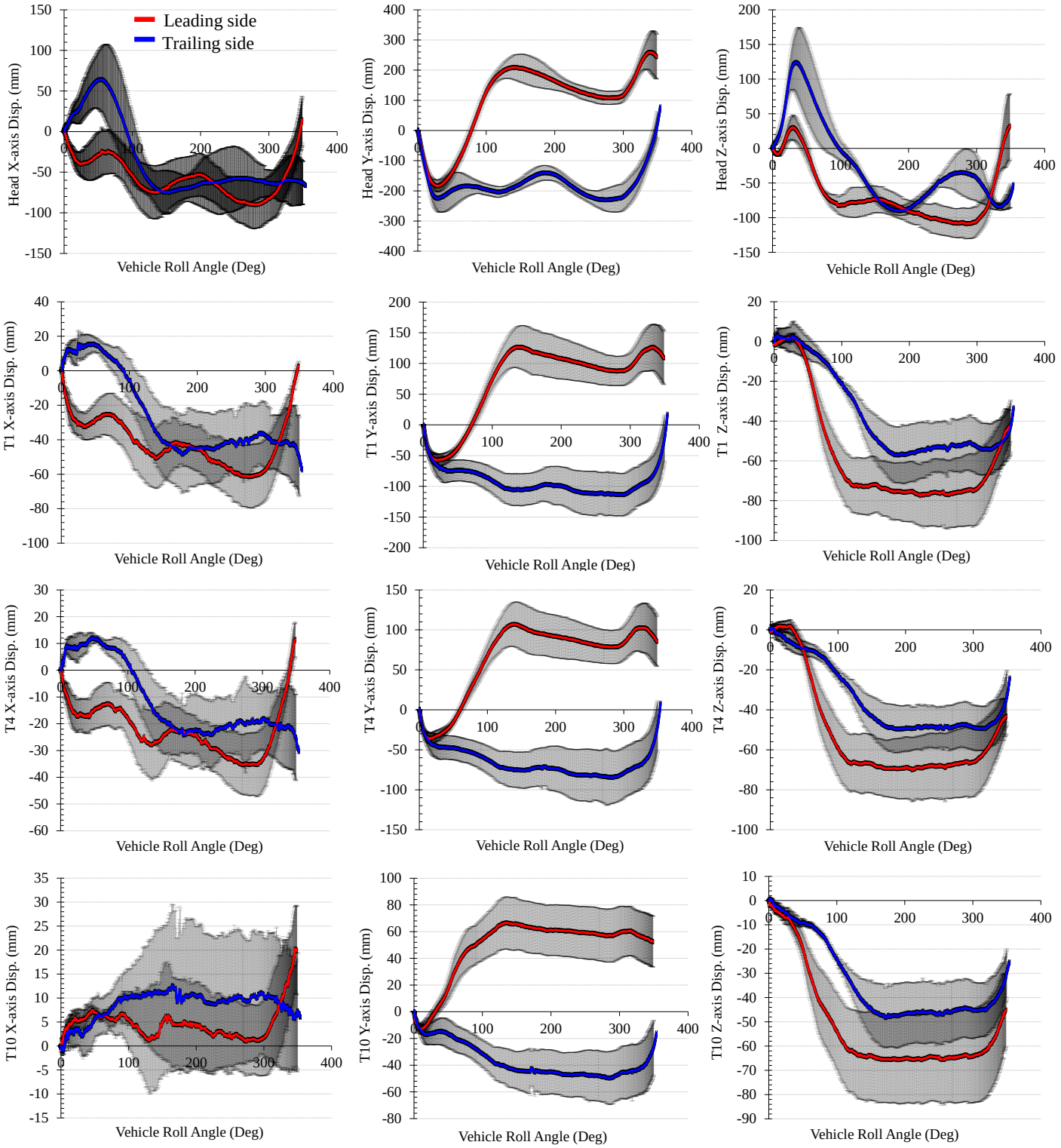

Figure 13. Head, T1, T4, and T10 displacements with respect to the vehicle buck.

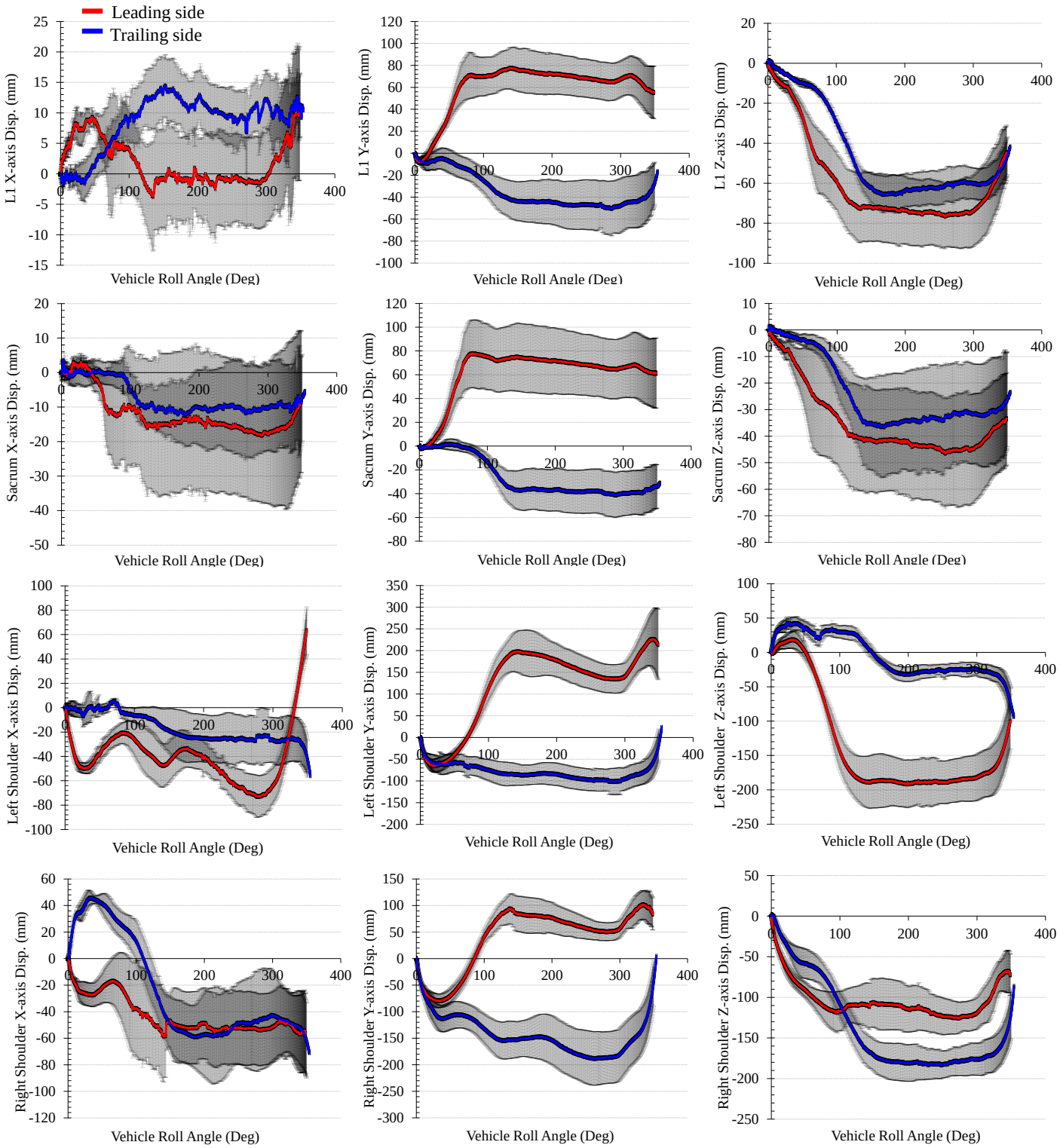

Figure 14. L1, sacrum, and shoulder displacements with respect to the vehicle buck.

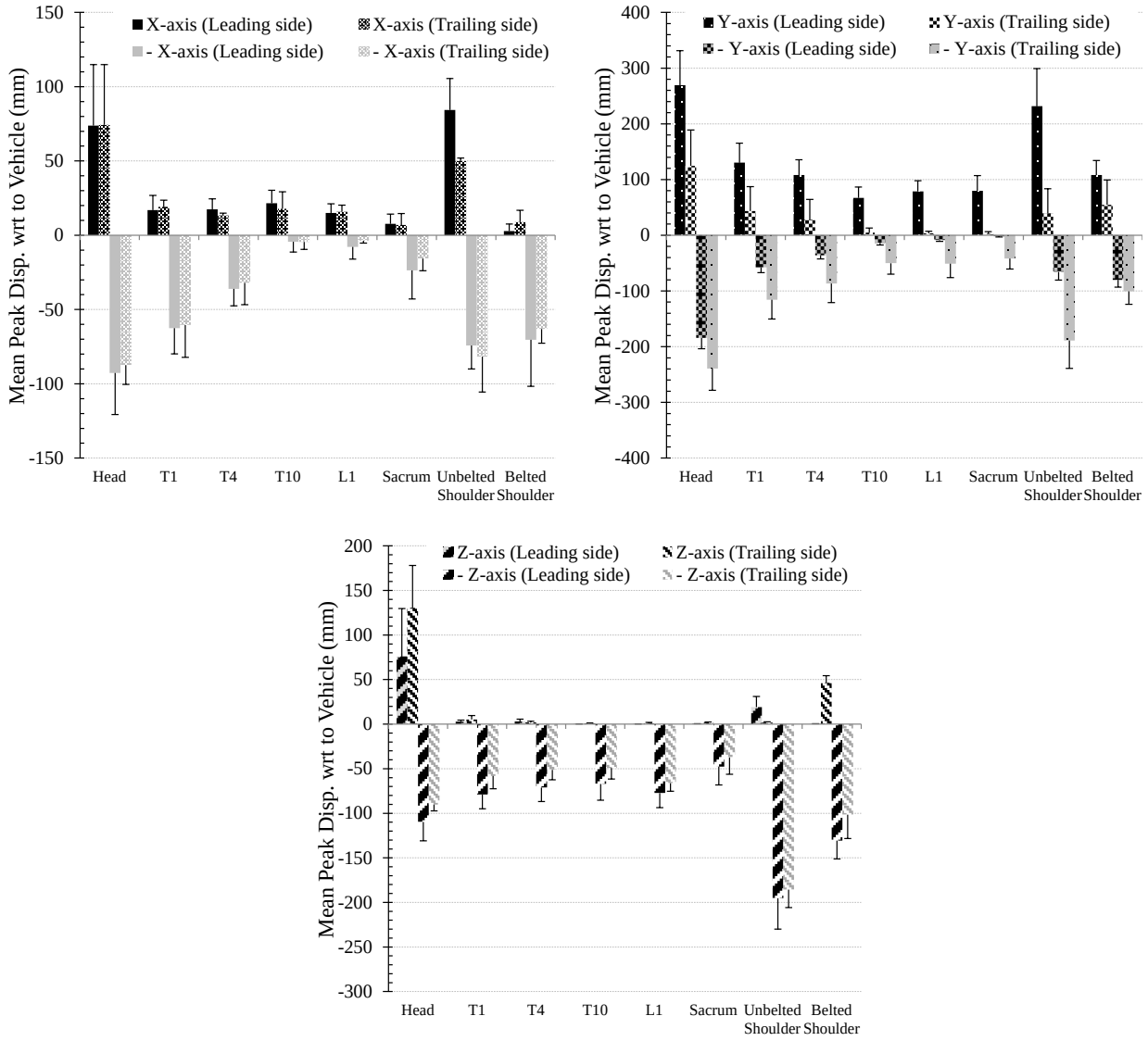

Figure 15. Mean peak X-,Y-, and Z-axis subject displacements ± 1 SD for leading-side and trailing-side seating positions. Peaks in both the positive and negative X-,Y-, and Z-axis directions are illustrated.

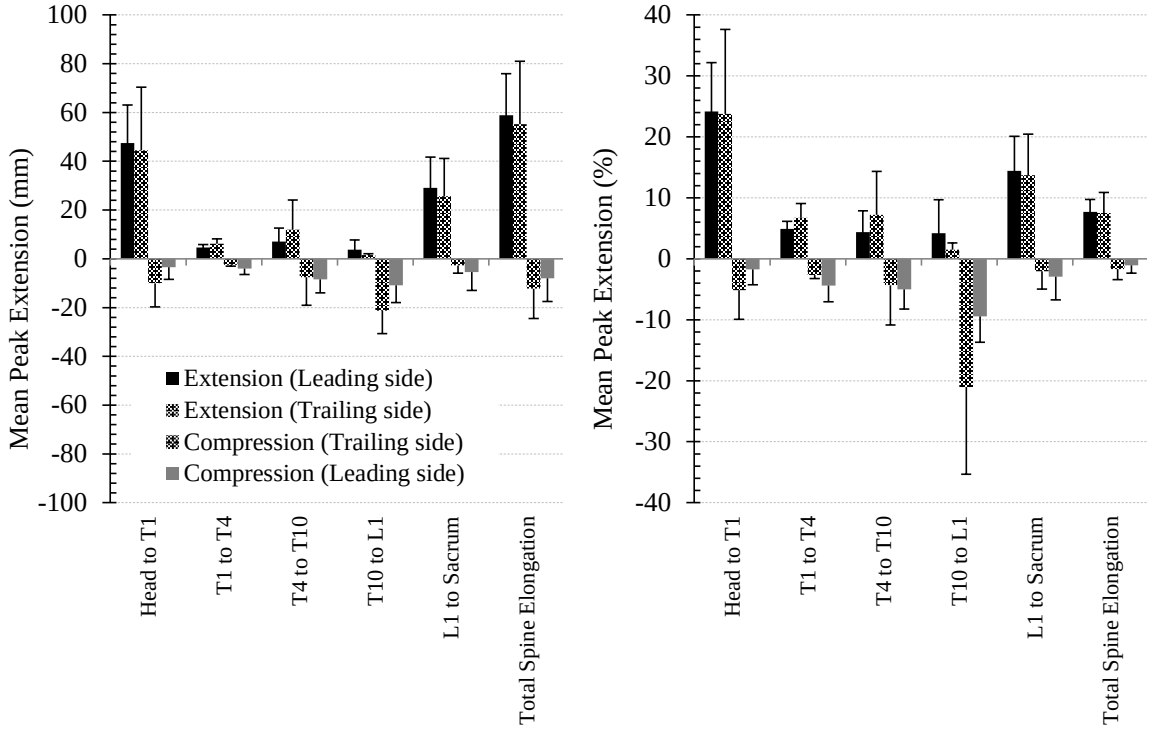

Figure 16. Mean peak spine segment extensions ± 1 SD for leading-side and trailing-side seat positions. Compression is indicated as negative extension.

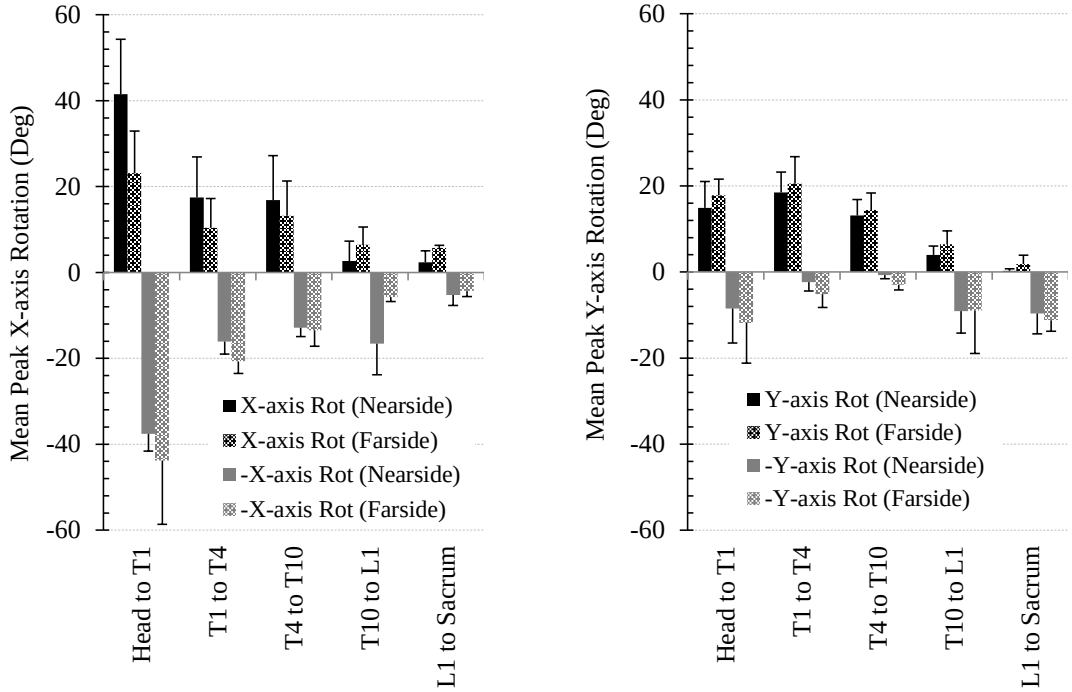

Figure 17. Mean peak spine segment rotations ± 1 SD for leading-side and trailing-side seat positions.

DISCUSSION

Kinematic Response Corridors

The primary objective of the current study was to characterize the whole-body kinematic response of PMHS in controlled laboratory rollover tests in order to generate foundational kinematic response targets. While effectively measuring occupant kinematics in the rollover environment has historically been challenging from a practical standpoint, the use of a measurement methodology incorporating 3D motion capture technology (Lessley et al., 2011) has now made it possible to quantify occupant motions that were largely impossible to measure with previously available methods. This approach provided detailed kinematic responses that included the 3D displacements of eight anatomical measurement locations as a function of vehicle roll angle. Additionally, the relative motion occurring between adjacent spinal measurement locations made it possible to characterize the extension, compression, and rotation of five separate segments along the length of the spine. For each occupant seating position (leading-side and trailing-side) 39 kinematic response corridors were successfully generated from the collected response data from the four tested PMHS.

The presented kinematic results generally demonstrated highly characteristic responses observed across all four tested PMHS. Referring to Figure 12, while some expected variation in the magnitude of a given measured parameter was observed, a nearly identical response shape and phase was often clearly observable and repeated across the tested subjects for a given kinematic response parameter . This was important for the generation of the response corridors. Since the individual responses shared similar phase and shape characteristics, the average of these responses naturally produced a characteristic average curve (Lessley et al., 2004) that was very representative of the individual response curves in terms of both phase and shape. This provided an effective, repeatable, and straightforward approach to construct a 1 SD corridor for a given response parameter. Thus, each final constructed corridor successfully captured the shape and phase characteristics of the individual PMHS responses while quantifying the inherent subject-to-subject variation around a characteristic average response. The produced collection of kinematic response targets provides a sound benchmark of PMHS performance in the tested condition.

Test-to-Test Repeatability

While previously conducted DRoTS tests with the Hybrid III 50th percentile male ATD demonstrated highly repeatable results (Zhang et al., 2013), it was desirable to evaluate test-to-test repeatability with PMHS, which are inherently more varied in terms of kinematic response. Figure 18 illustrates and example of PMHS test-to-test repeatability in the leading-side seating position for the T1 measurement location, which was a primary measurement site for characterizing both lateral and vertical motions of the occupant torso. A single repeated test was performed with subjects 2, 3, and 4 (Table 1), for which T1 Y- and Z-axis displacement data is illustrated in each column of Figure 18. Generally, the repeated test results mimicked the results obtained from all four PMHS, in that the shape and phase of the repeated tests were nearly identical, while some variation in the magnitude of the response was observed. This variation in magnitude was, however, substantially less than the overall variation in displacement magnitude across the four tested PMHS. Referring to Figure 18, the difference in peak displacement between repeated tests was 12.4 percent of the mean peak displacement value, on average for the illustrated T1 Y- and Z-axis displacements. While this variation in the PMHS, was greater than for the Hybrid III ATD (Zhang et al., 2013), it is similar to the variation reported by Moffatt et al. (1997) for repeated rollover tests with human subjects. More generally, across the X-, Y-, and Z-axis displacements for the all eight measurement locations (Figure 6), the SD in repeated tests was, on average, approximately half of that observed across all four PMHS. Thus, for a selected measurement parameter, the response curve for a repeated test naturally fell within the range of responses from the four tested PMHS.

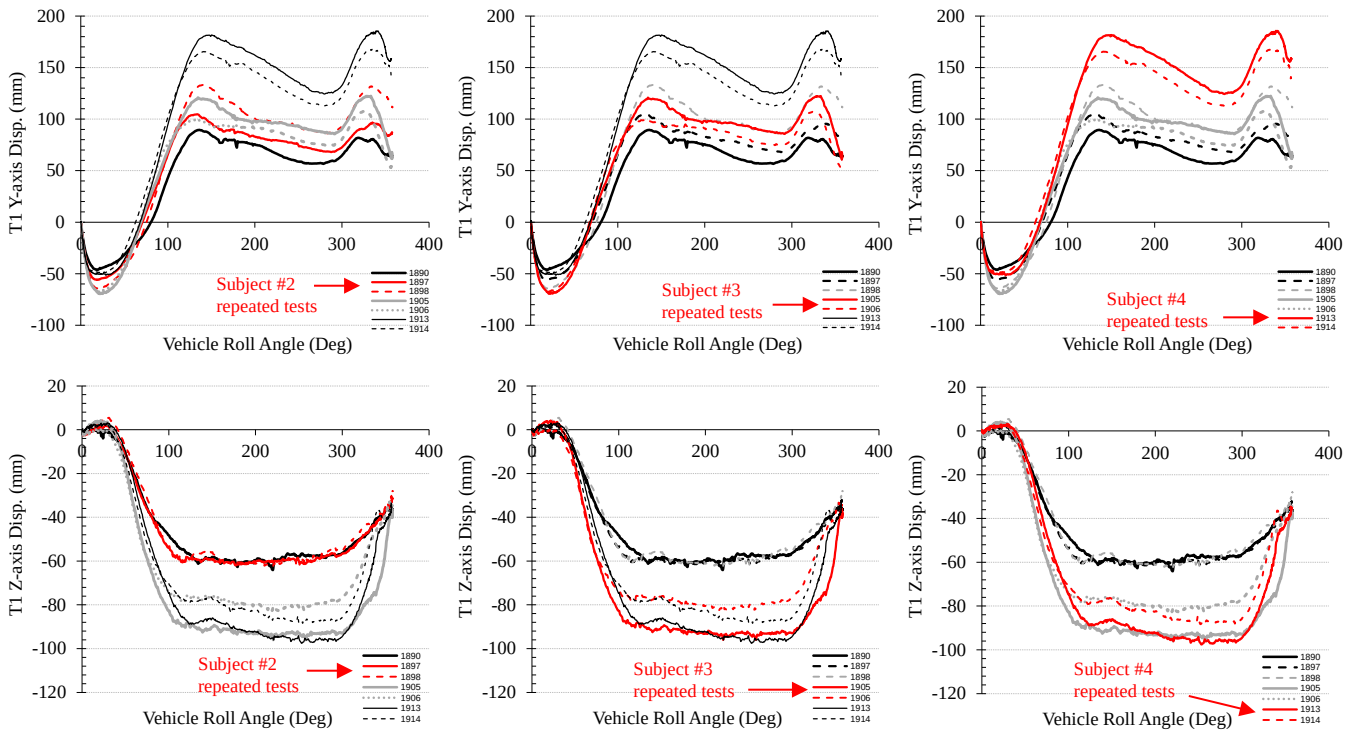

Figure 18. Test-to-test repeatability for a given PMHS for the T1 measurement location.

Kinematic Observations

Regardless of seating position, the head and torso measurement locations generally moved outboard (positive Y-axis for leading-side and negative Y-axis for trailing-side) and upward (negative Z-axis) during the rollover event, with locations superior to T10 also moving rearward (negative X-axis)(Figure 19). The centrifugal forces, occurring during the rollover event, displaced the occupant both upward and outboard with the final position being limited primarily by the belt restraints and structure of the vehicle interior. Similar upward and outboard occupant motions have been observed in previous studies (Bahling et al., 1990; Orlowski et al., 1985). Furthermore, separation between the PMHS and the seat pan occurred early in the event and was maintained until the end of the test, which is similar to the observation reported by Bahling et al. (1990) for tests with ATDs.

Referring to Figure 15, lateral occupant displacements were the greatest at superior locations and gradually decreased in magnitude with increasingly inferior locations. For locations superior to T10, occupant displacements in the lateral (Y-axis) direction were substantially greater in magnitude than were displacements in either the X- or Z-axis directions. For locations inferior to T10, the Y-axis and Z-axis displacements were similar in magnitude. Likewise, spine segments rotated laterally outboard with superior locations exhibiting greater rotations than inferior locations.

The PMHS also displaced rearward at locations superior to the T10 level (Figure 19). This occurred as the PMHS spine straightened to align with the forces generated from the combined radial and gravitational accelerations. This resulted in spine segments superior to T10 predominately rotating rearward, while those inferior to T10 predominately rotated forward (Appendix A). Forces acting on the PMHS spines were generally found to extend (i.e. elongate) the spine during the tests, with the greatest extensions occurring in the cervical and lumbar segments, while the T10 to L1 segment consistently experienced compression (Figure 16). Overall, the spine elongated during the tests by a total of 59 mm and 55 mm in the leading-side and trailing-positions respectively (Figure 16).

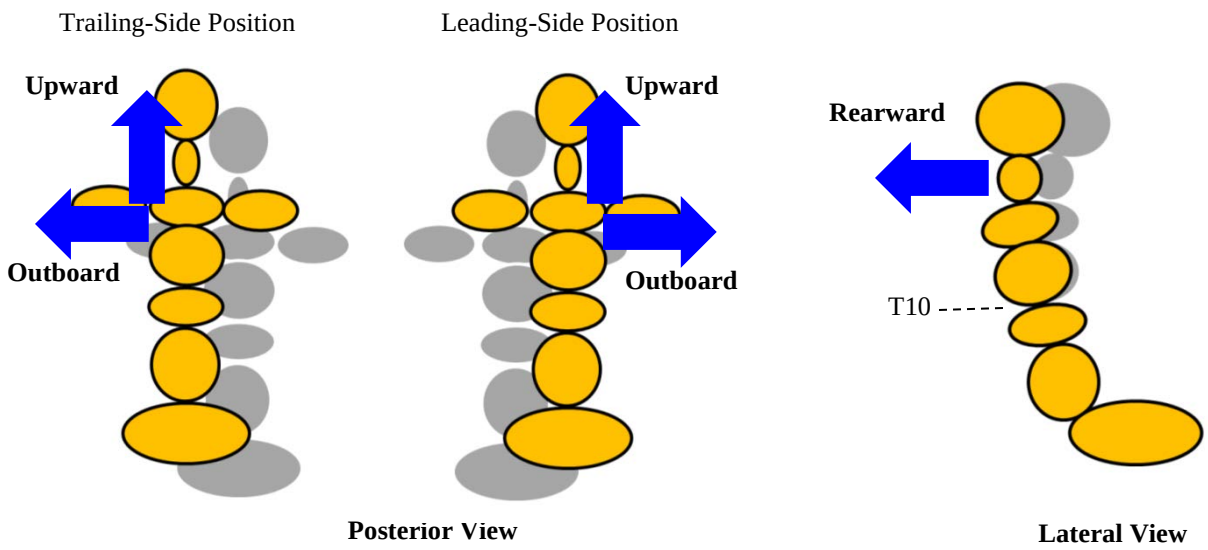

Figure 19. Predominant occupant motions.

Leading-Side vs. Trailing-Side Response

Comparison of PMHS responses in leading-side and trailing-side occupant seating positions revealed both similarities and differences that were repeated across the four tested PMHS. The kinematic response trends described above were consistently observed regardless of seating position. In contrast, however, other kinematic responses differed substantially between occupant seating positions. One of the most important differences in kinematic response between seating positions occurred for upward (negative Z-axis) displacement. Substantially greater upward displacements were consistently observed for the leading-side seating position. The peak upward displacement of T1 was 36% greater on average for the leading-side seating position than that for the trailing-side position. A similar increase in upward displacement was observed at all measurement locations, which averaged 26% greater peak vertical displacement for the leading-side than for the trialing-side positions (Figure 20). The location that showed the largest difference in upward displacement throughout the entire event was the belted shoulder (outboard shoulder that the belt passed over). Figure 21 illustrates the upward displacements of the belted shoulder and T1 in both seating positions. The belted shoulder in the leading-side position displaced upwardly throughout the entire rollover event, while the trailing-side belted shoulder failed to displace in an upward direction until approximately 150 degrees of vehicle roll angle. The early and greater upward displacement of the belted shoulder in the leading-side position led to both an earlier and greater upward displacement of T1 which was propagated to all other measurement locations along the spine, which is clearly illustrated in the Z-axis displacements in Figures 13 and 14. Similarly, the lateral outboard displacements were also greater for the leading-side position which were 32% greater on average than those for the trailing-side position (Figure 20).

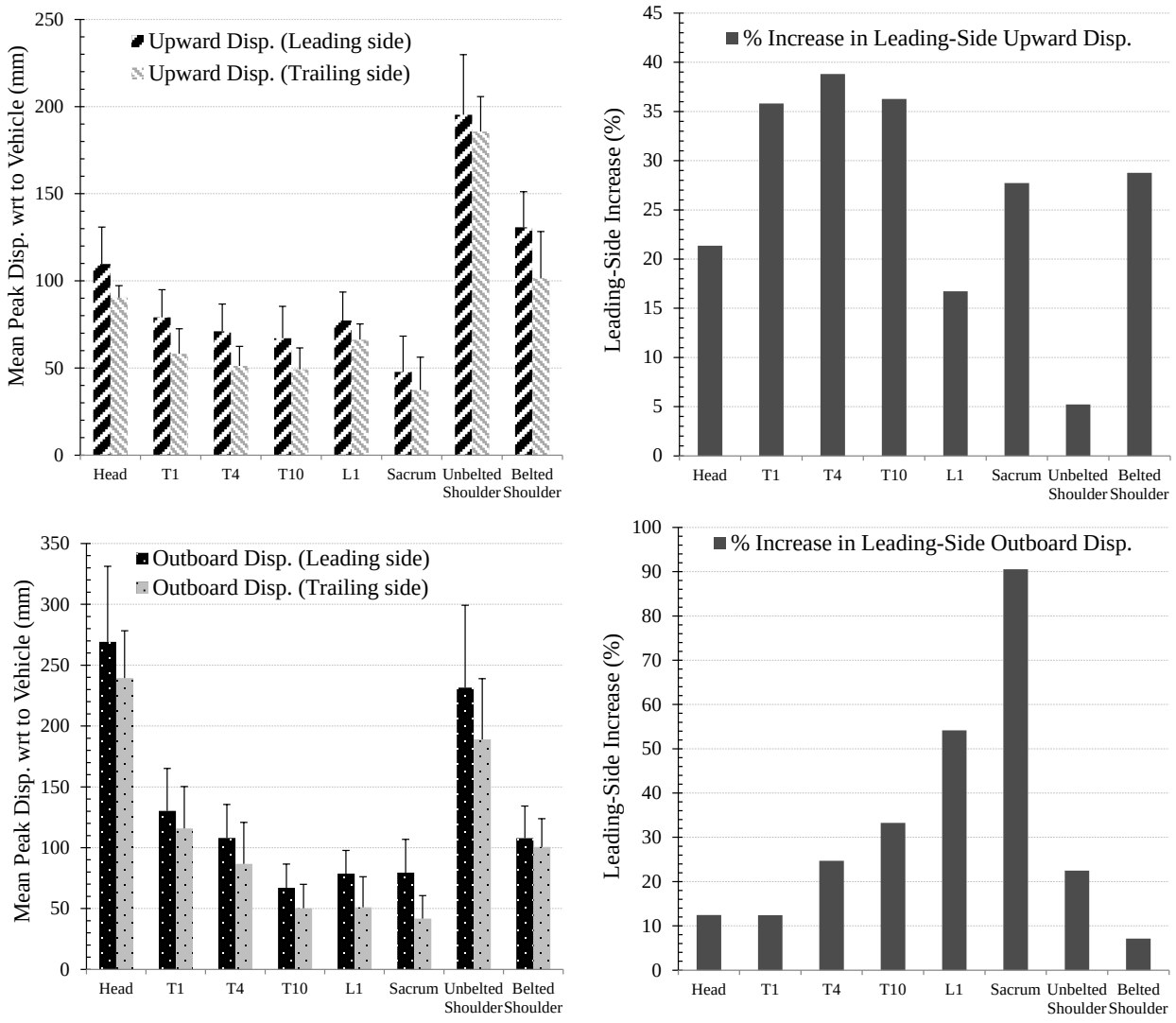

Figure 20. Leading-side vs. trailing-side mean peak upward and outboard displacements.

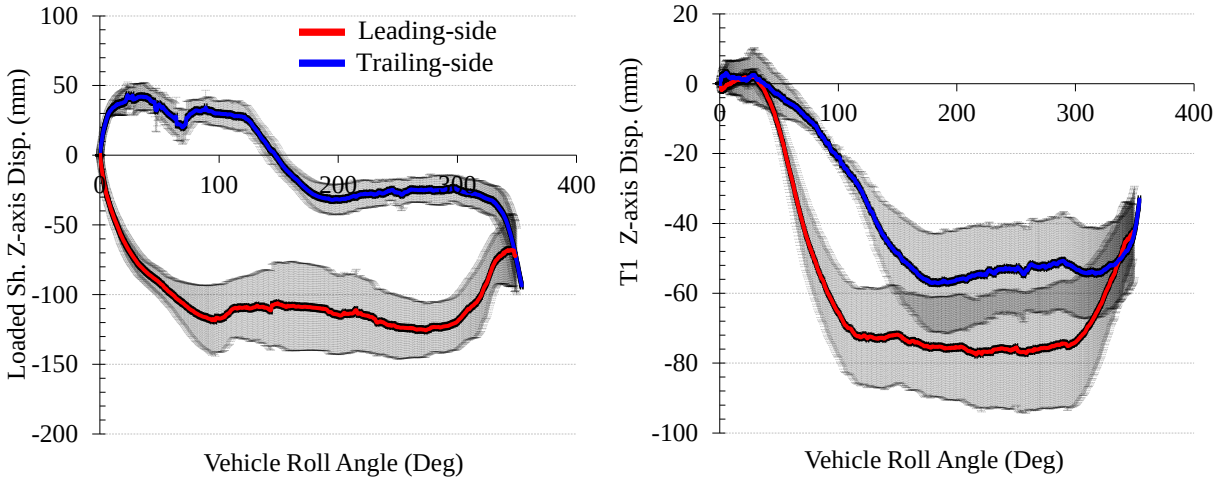

Figure 21. Leading-side vs. trailing-side mean peak upward displacement corridors.

PMHS Response Relative to Previous Studies

The general upward and outboard occupant displacements exhibited in both seating positions are similar to those observed in previously reported rollover studies (Bahling et al., 1990; Orlowski et al., 1985). Interestingly, however, the greater upward displacement for the leading-side occupant in the current study is in contrast to the findings reported by Moffatt et al. (2003) where it was the trailing-side occupant that experienced the greatest upward displacement. Given the considerable difference in occupant displacement behavior across seating positions in the two studies (i.e. the current study and Moffatt et al., 2003), it is necessary to investigate why this difference occurred, especially given the consistency of the occupant behavior within a given study.

Moffatt et al. (2003) reported that the trailing-side occupant leaned laterally inboard, which allowed the outboard shoulder to slip out from under the belt. This in turn allowed for more upward displacement of the trailing-side occupant. For the leading-side occupant, no such inboard lean or shoulder belt slip was noted, and thus the upward displacement of the leading-side occupant was less than that for the trailing-side occupant.

In the current study, early in the rollover event (during the first quarter turn) the opposite trend occurred, where it was the leading-side occupant that leaned laterally inboard away from the shoulder belt and vehicle door, while the trailing-side occupant leaned outboard into the shoulder belt and vehicle door (Figures 13, 14, and 22). Figure 22 clearly illustrates the inboard lean occurring for the leading-side position, and also the outboard lean in the trailing-side position where the PMHS maintained door contact, even at a 90 degree roll angle. In the current study, the less effectively restrained leading-side occupant experienced substantially more (28% on average) upward displacement during the rollover event.

Leading-Side Position *45° Vehicle Roll Angle* **Inboard lean, no door contact**	**Trailing-Side Position** *45° Vehicle Roll Angle* **Outboard lean, door contact**	**Trailing-Side Position** *90° Vehicle Roll Angle* **Outboard lean, door contact**

Figure 22. PMHS inboard and outboard occupant lean for the current study for leading-side and trailing-side seating positions.

It is apparent from both studies that the occupant that leaned inboard away from the shoulder belt and door also experienced greater upward displacement. Thus, it is the initial lateral lean that is related to the upward displacement in the same way in both studies. However, what is most interesting is the fact that the occupants initially leaned laterally in opposite directions in the two studies (Figure 22). That is, early on the occupants in the current study leaned toward the occupants' left, while in the Moffatt et al. (2003) study the occupants initially leaned toward the occupants' right. The explanation for this response difference is the difference in the angular acceleration, α, used in the two studies.

While the peak roll rate was comparable across the two studies, the angular acceleration differed considerably between the Moffat et al. (2003) study and the current study. In the Moffatt et al. (2003) study peak roll rate was reached after approximately three full revolutions (1080 degrees), where in the current study peak roll rate was achieved in one third of a revolution (125 degrees), which is more similar, yet still lower, than angular accelerations resulting from steering induced vehicle rollovers (Asay and Woolley, 2009; Asay and Woolley, 2010). Thus, the average rotational acceleration was approximately 14 times greater in the current study than that used by Moffatt et al. (2003). This greater rotational acceleration initially caused both occupants to lean, relative to the vehicle, toward the occupants' left due to inertial forces. In contrast, the lower rotational acceleration used by Moffatt et al. (2003) did not produce such large inertial forces. Instead, the occupants initially leaned, relative to the vehicle, toward the occupants' right due to gravitational forces. Thus, as Figure 23 illustrates, in the current study (with large α) the initial lateral motions to the left were produced by inertial forces arising from the large rotational acceleration, while in the Moffett et al. (2003) study (with smaller α), initial lateral motions to the right were produced by the force of gravity. Ultimately, once inboard motion away from the shoulder belt and door occurred in either study, the affected occupant experienced a greater upward displacement during the rollover event. Thus, both studies accurately and consistently observed a specific kinematic behavior that was related to a given seating position, however, the characteristics of the observed kinematic behavior clearly differ with changes in rotational acceleration. This finding highlights the importance of rotational acceleration on occupant response as well as the restraining effect of occupant interaction with the interior surface of the vehicle door.

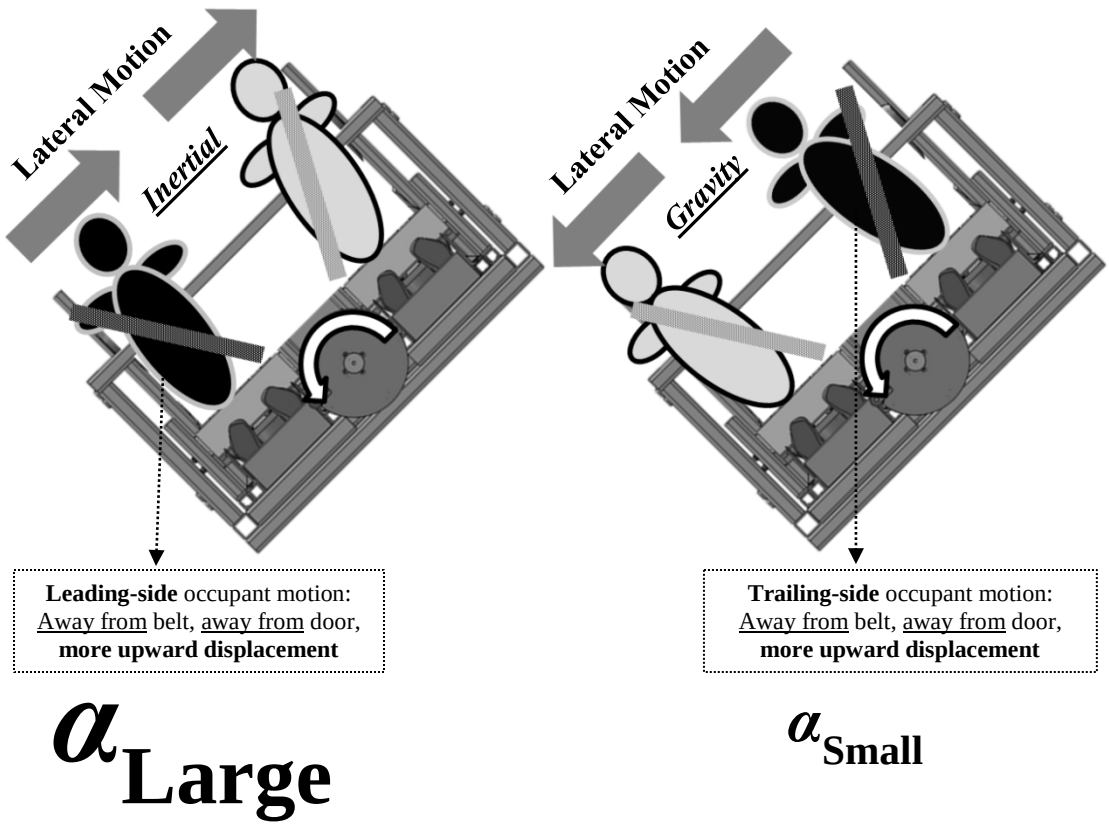

Figure 23. Effect of rotational acceleration (α) on occupant kinematics in leading-side and trailing-side seating positions.

CONCLUSION

The current study characterized the whole-body kinematic response of four PMHS in controlled laboratory rollover tests (without ground contact) for both the leading-side and trailing-side occupant seating positions. The kinematic results generally demonstrated highly characteristic responses observed across all four tested PMHS which enabled a total of 78 kinematic response corridors to be generated.

Regardless of seating position, the head and torso measurement locations generally moved outboard and upward during the rollover event, with locations superior to T10 also moving rearward. The PMHS spines were generally found to elongate during the tests, with the greatest extensions occurring in the cervical and lumbar segments, while the T10 to L1 segment consistently experienced compression. Substantially greater upward and outboard displacements were consistently observed for the leading-side seating position. Due to inertial effects arising from rotational acceleration, the leading-side occupant initially leaned laterally inboard away from the shoulder belt and vehicle door, while the trailing-side occupant leaned outboard into the shoulder belt and vehicle door. This initial lateral motion (inboard for the leading-side occupant and outboard for the trailing-side occupant) caused the leading-side occupant to be less effectively restrained which led to substantially more (28% on average) upward displacement during the rollover event compared to the more effectively restrained trailing-side occupant. This finding highlights the importance of rotational acceleration on occupant response as well as the restraining effect of occupant interaction with the interior surface of the vehicle door. The reported data represent the most complete set of kinematic response targets for a restrained occupant in a dynamic rollover condition, and are immediately useful for efforts to evaluate and improve existing ATDs and computational models for use in the rollover crash environment.

ACKNOWLEDGEMENTS

This study was supported by the National Highway Traffic Safety Administration (NHTSA) under Cooperative Agreement No. DTNH22-09-H-00247. Views or opinions expressed or implied are those of the authors and are not necessarily representative of the views or opinions of the NHTSA.

REFERENCES

ANDERSON, T. E. (1974) Passenger Compartment Intrusion in Automobile Accidents. DOT HS-801 238, Final Report.

ARNDT, M. W., MOWRY, G. A., DICKERSON, C. P., ARNDT, S. M. (1995) Evaluation of Experimental Restraints in Rollover Conditions. SAE 952712.

ASAY, A. F., WOOLLEY, R. L. (2010) Rollover Testing of Sport Utility Vehicles (SUVs) on an Actual Highway. SAE 2010-01-0521.

ASAY, A. F., WOOLLEY, R. L. (2009) Rollover Testing on an Actual Highway. SAE 2009-01-1544.

BAHLING, G. S., BNUDORF, R. T., KASPZYK, G. S., MOFFATT, E. A., ORLOWSKI, K. F., STOCKE, J. E. (1990) Rollover and Drop Tests – The Influence of Roof Strength on Injury Mechanics Using Belted Dummies. SAE 902314.

CAMPBELL, B. J. (1962) Seat Belts in Convertible Car Accidents. Automotive Crash Injury Research of the Cornell Aeronautical Laboratory, Inc., Bulletin Number 3.

EVANS, L. (1988). Restraint Effectiveness, Occupant Ejection from Cars, and Fatality Reductions. General Motors Research Laboratories, GMR-6398.

FOLTZ, P., KIM, T., KERRIGAN, J. R., CRANDALL, J.R. (2011) Vehicle greenhouse shape analysis for design of a parametric test buck for dynamic rollover testing. Proceedings of 22nd International Conference on the Enhanced Safety of Vehicles (ESV), Paper Number 11-0271.

HERBST, B., FORREST, S., WANG, P., CHNG, D., FRIEDMAN, D., FRIEDMAN, K. (1996) The Ability of Three-point Safety Belts to Restrain Occupants in Rollover Crashes. 15th International Technical Conference on Experimental Safety of Vehicles.

HIGHT, P. V., SIEGLE, A.W., NAHUM, A.M. (1972) Injury Mechanisms in Rollover Collisions. Proceedings of the 16th Stapp Car Crash Conference.

HUELKE , D. F., LAWSON, T. E., MARSH, J. C. (1977a). Injuries, Restraints, and Vehicle Factors in Rollover Car Crashes. Accident Analysis and Prevention, 9:93-107.

HUELKE, D. F., LAWSON, T. E., SCOTT, R., MARSH, J. C. (1977b). The Effectiveness of Belt Systems in Frontal and Rollover Crashes. SAE 770148.

HUELKE, D.F., MARSH, J.C., DIMENTO, L.J., SHERMAN, H.W., AND BALLARD, W.J. (1973) Injury Causation in Rollover Accidents. Proceedings of the 17th Conference of the American Association for Automotive Medicine.

HUELKE, D. F., MARSH, J. C., SHERMAN, H. W. (1972) Analysis of Rollover Accident Factors and Injury Causation. 16th Conference of the American Association for Automotive Medicine.

JAMES, M. B., ALLSOP, D. L., NORDHAGEN, R. P., DECKER, R. L. (1997) Injury Mechanisms and Field Accident Data Analysis in Rollover Accidents. SAE 970396.

KERRIGAN J. R., JORDAN, A., PARENT, D., ZHANG, Q., FUNK, J., DENNIS, N. J., OVERBY, B., BOLTON, J., CRANDALL, J. (2011) Design of a dynamic rollover test system, Society of Automotive Engineers, SAE 2011-01-1116.

LESSLEY, D. J., CRANDALL, J. R., SHAW, C. G., KENT, R. W., FUNK, J. R. (2004) A Normalization Technique for Developing Corridors from Individual Subject Responses. SAE 2004-01-0288.

LESSLEY, D., SHAW, G., PARENT, D., ARREGUI-DALMASES, C., KINDIG, M., RILEY, P., PURTSEZOV, S., SOCHOR, M., GOCHENOUR, T., BOLTON, J., SUBIT, D., CRANDALL, J., TAKAYAMA, S., ONO, K., KAMIJI, K., YASUKI, T. (2010) Whole-Body Response to Pure Lateral Impact. Stapp Car Crash Journal,54:289-336.

LESSLEY, D., SHAW, G., RILEY, P., FORMAN, J., CRANDALL, J. (2011) Assessment and Validation of a Methodology for Measuring Anatomical Kinematics of Restrained Occupants During Motor Vehicle Collisions. J Biosens Bioelectron S1:002. doi: 10.4172/2155-6210.S1-002.

LOPEZ-VALDES, F. J., LAU, A., LAMP, J., RILEY, P. O., LESSLEY, D. J., DAMON, A., KINDIG, M., KENT, R. W., BALASUBRAMANIAN, S., SEACRIST, T., MALTESE, M. R., ARBOGAST, K. B., HIGUCHI, K., TANJI, H. (2010) Analysis of Spinal Motion During Frontal Impacts. Comparison between PMHS and ATD. Proc. of the Association for the Advancement of Automotive Medicine. 54:61-78.

FORMAN, J., LOPEZ-VALDES, F., LESSLEY, D., RILEY, P., SOCHOR, M., HELTZEL, S., ASH, J., PERZ, R., KENT, R., SEACRIST, T., ARBOGAST, K., TANJI, H., HIGUCHI, K. (2013). Occupant Kinematics and Shoulder Belt Retention in Far-Side Lateral and Oblique Collisions: A Parametric Study. Stapp Car Crash Journal, 57: 343-85.

MOFFATT, E. A., COOPER, E. R., CROTEAU, J. J., PARENTEAU, C., TOGLIA, A. (1997) Head Excursion of Seat Belted Cadaver, Volunteers, and Hybrid III ATD in a Dynamic/Static Rollover Fixture. SAE 973347.

MOFFATT, E., HARE, B., HUGHES, R., LEWIS, L., IIYAMA, H., CURZON, A., COOPER, E. (2003) Head Excursion of Restrained Human Volunteers and Hybrid III Dummies in Steady State Rollover Tests. 47th Annual Proceedings for the Association for the Advancement of Automotive Medicine.

National Highway Traffic Safety Administration (NHTSA). (2010) Traffic Safety Facts 2008—A Compilation of Motor Vehicle Crash Data from the Fatality Analysis Reporting System and the General Estimate System. Early Edition. DOT HS 811 170. http://www-nrd.nhtsa.dot.gov/Pubs/811170.PDF

ORLOWSKI, K. F., BUNDORF, R. T., MOFFATT, E. A. (1985) The Influence of Roof Strength on Injury Mechanics. SAE 851734.

PYWELL, J. F., ROUHANA, S. W., MCCLEARY, J. D., DESAELE, K. H. (1997) Characterization of Belt Restraint Systems in Quasistatic Vehicle Rollover tests. SAE 973334.

SCHNEIDER, L. W., ROBBINS, D. H., PFLUG, M. A., SNYDER, R. G. (1983) Anthropometry of Motor Vehicle Occupants, Vol. 3. Specifications and Drawings. Report HS-806 717; UMTRI-83-53-2, UMTRI.

Society of Automotive Engineers. (1994) SAE Surface Vehicle Information Report: Sign Convention for Vehicle Crash Testing . SAE J1733.

SHAW, G., PARENT, D., PURTSEZOV, S., LESSLEY, D., CRANDALL, J., KENT, R., GUILLEMOT, H., RIDELLA, S. A., TAKHOUNTS, E., MARTIN, P. (2009) Impact Response of Restrained PMHS in Frontal Sled Tests: Skeletal Deformation Patterns Under Seat Belt Loading. Stapp Car Crash Journal, 53: 1-48.

SHOEMAKER, N. E. (1959). Study of Human Kinematics in a Rolled Over Automobile. Cornell Aeronautical Laboratory, Inc., Report No. YM-1246-D-1.

STONE, K. (1974) Occupant Protection During Vehicle Rollover. 5th International Technical Conference on Experimental Safety of Vehicles.

WARD, C. C, DER AVANESSIAN, H., WARD, P., PAVER, J. G. (2001) Investigation of Restraint Function on Male and Female Occupants in Rollover Events. SAE 2001-01-0177.

APPENDIX

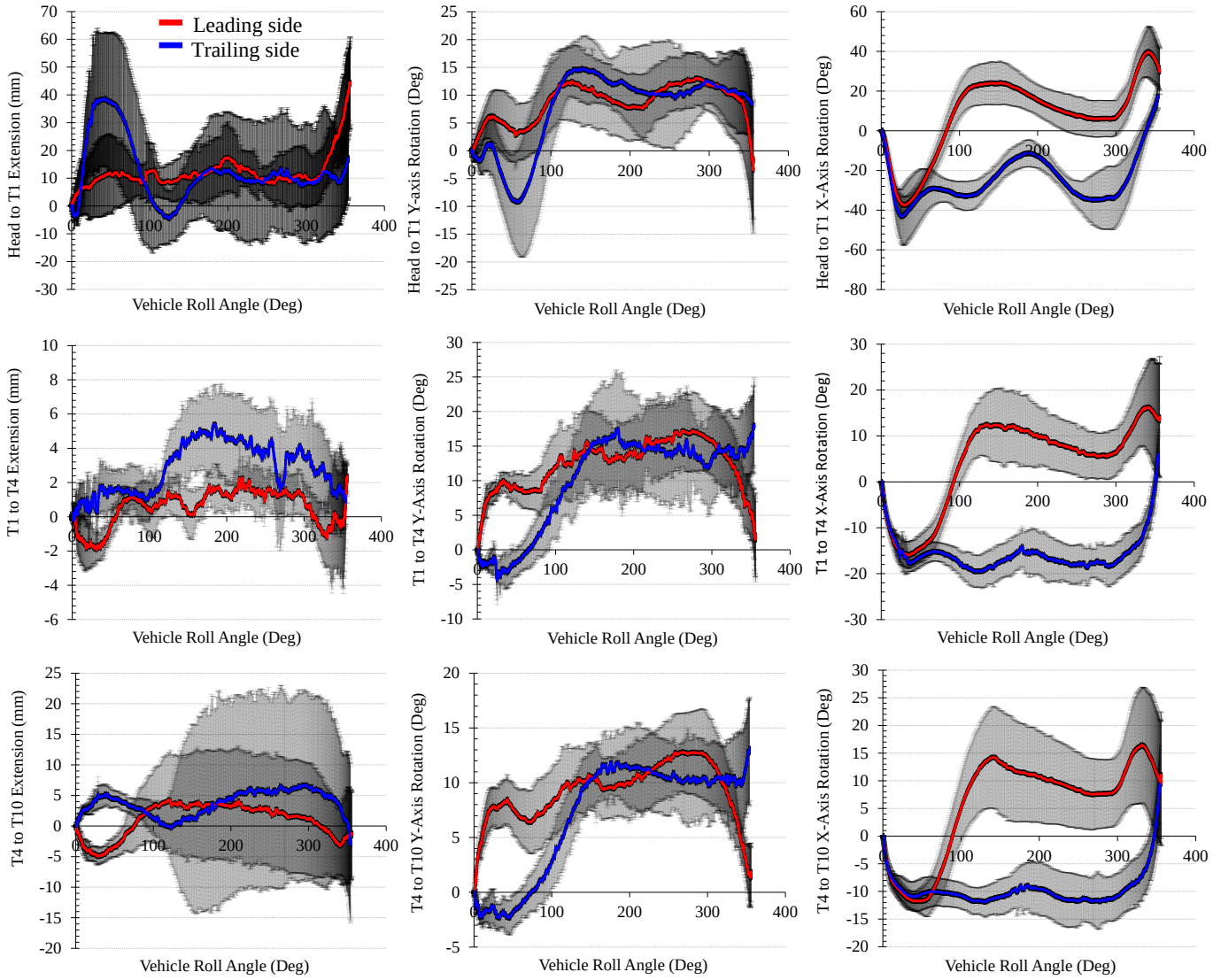

Figure A1. Segment extension and rotations for head to T1, T1 to T4, and T4 to T10 spine segments.

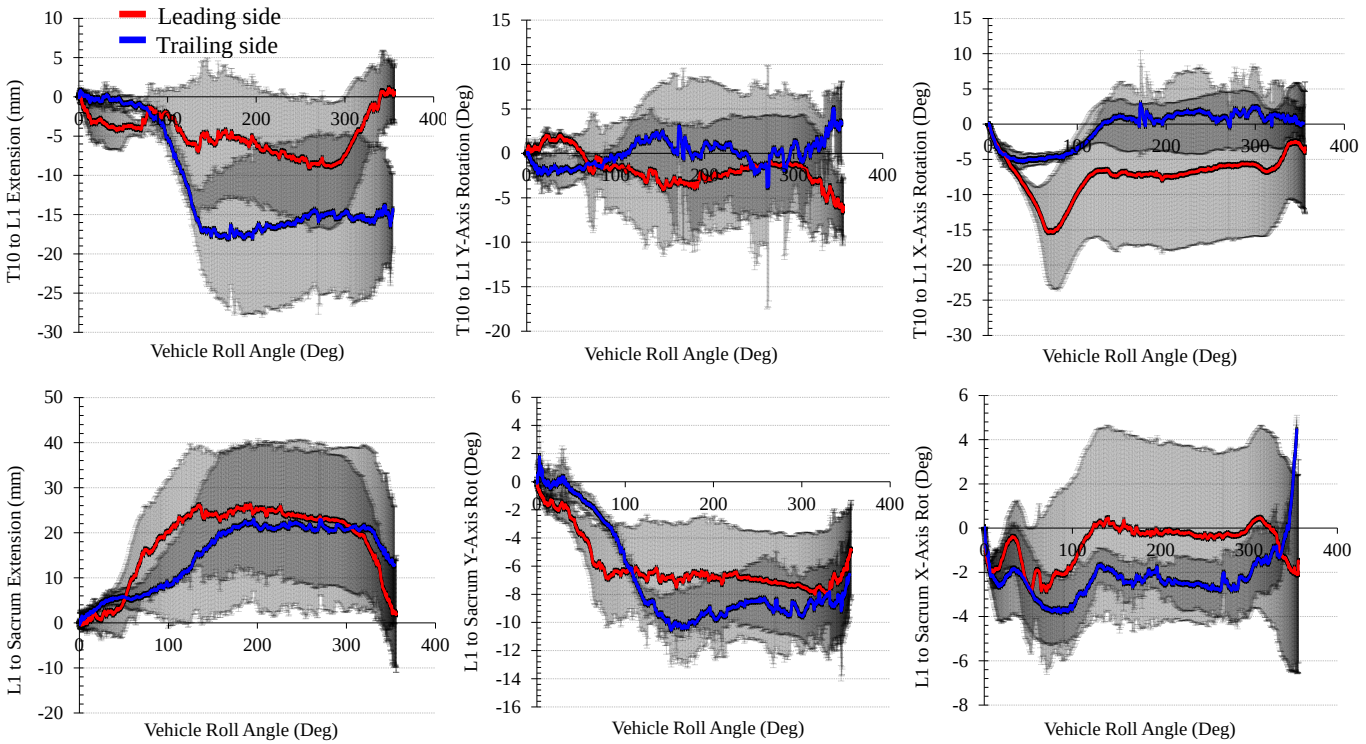

Figure A2. Segment extension and rotations for T10 to L1 and L1 to sacrum spine segments.

Table A1. Summary of Peak Values for PMHS Displacement with Respect to the Vheicle Buck for Leading-Side and Trailing-Side Positions.

			Leading-Side										Trailing-Side						
			1890	**1897**	**1898**	**1905**	**1906**	**1913**	**1914**	**COV**	**SD**	**AVE**	**AVE**	**SD**	**COV**	**1894**	**1902**	**1910**	**1918**
Head	X-axis	pos	113.0	37.3	21.3	54.8	61.6	95.2	133.2	0.6	41.1	**73.8**	**74.3**	40.6	0.5	117.5	36.1	43.3	100.2
	(mm)	neg	-83.9	-99.5	-116.8	-63.5	-56.2	-135.7	-92.8	0.3	28.1	**-92.6**	**-87.4**	13.0	0.1	-92.1	-103.6	-78.6	-75.3
	Y-axis	pos	261.0	247.9	306.8	210.1	180.3	336.7	341.5	0.2	62.1	**269.2**	**124.5**	64.4	0.5	171.0	106.5	41.2	179.4
	(mm)	neg	-178.3	-170.4	-178.6	-175.5	-169.3	-224.3	-193.8	0.1	19.4	**-184.3**	**-239.4**	38.9	0.2	-296.3	-213.3	-232.4	-215.5
	Z-axis	pos	123.0	46.3	54.6	10.1	26.2	130.1	140.4	0.7	54.0	**75.8**	**130.5**	47.6	0.4	184.9	125.0	69.9	142.2
	(mm)	neg	-106.6	-94.8	-89.9	-115.1	-90.8	-149.3	-120.8	0.2	21.2	**-109.6**	**-90.3**	6.9	0.1	-82.3	-88.2	-92.0	-98.8
T1	X-axis	pos	19.1	11.7	1.2	14.6	13.6	28.3	29.8	0.6	9.9	**16.9**	**19.0**	4.6	0.2	16.4	13.9	23.3	22.5
	(mm)	neg	-52.7	-67.7	-84.6	-44.3	-40.1	-81.3	-67.0	0.3	17.4	**-62.5**	**-60.5**	21.7	0.4	-52.5	-84.0	-34.3	-71.1
	Y-axis	pos	89.5	104.6	133.1	122.3	108.2	185.6	167.9	0.3	35.0	**130.2**	**43.3**	43.8	1.0	36.3	29.8	2.0	105.1
	(mm)	neg	-46.4	-56.0	-64.3	-69.5	-67.6	-51.5	-49.2	0.2	9.3	**-57.8**	**-115.8**	34.4	0.3	-92.0	-118.8	-163.4	-89.1
	Z-axis	pos	0.4	2.4	5.5	4.1	0.4	3.1	3.1	0.7	1.9	**2.7**	**5.1**	4.6	0.9	0.8	10.3	1.7	7.6
	(mm)	neg	-64.1	-61.9	-62.5	-96.0	-82.7	-97.5	-88.4	0.2	15.9	**-79.0**	**-58.2**	14.3	0.2	-57.3	-39.0	-63.6	-72.8
T4	X-axis	pos	10.5	23.9	20.6	11.1	8.9	25.7	21.4	0.4	7.0	**17.4**	**13.3**	1.6	0.1	13.2	11.7	15.5	12.8
	(mm)	neg	-26.9	-34.9	-45.6	-22.4	-26.8	-53.5	-42.2	0.3	11.5	**-36.0**	**-32.1**	14.7	0.5	-23.3	-44.3	-16.1	-44.7
	Y-axis	pos	79.0	78.6	100.5	107.7	101.6	151.0	137.9	0.3	27.5	**108.0**	**27.9**	36.4	1.3	9.7	20.9	0.1	81.1
	(mm)	neg	-25.7	-37.1	-44.0	-41.4	-39.9	-32.5	-31.5	0.2	6.4	**-36.0**	**-86.6**	34.2	0.4	-62.7	-82.2	-136.3	-65.5
	Z-axis	pos	2.8	2.1	7.2	0.1	0.2	4.9	3.4	0.9	2.5	**3.0**	**1.8**	1.5	0.8	0.1	2.1	1.4	3.7
	(mm)	neg	-55.6	-56.5	-53.9	-92.5	-78.6	-84.4	-76.2	0.2	15.6	**-71.1**	**-51.2**	11.2	0.2	-52.0	-35.2	-58.1	-59.6
T10	X-axis	pos	9.3	28.7	35.3	20.9	17.1	24.4	15.4	0.4	8.7	**21.6**	**17.8**	11.4	0.6	13.7	18.0	33.3	6.3
	(mm)	neg	-0.6	-0.1	-0.2	-1.5	-0.2	-17.0	-11.3	1.6	6.9	**-4.4**	**-4.6**	4.9	1.1	-4.4	-0.8	-1.4	-11.5
	Y-axis	pos	73.1	36.7	42.7	87.7	77.5	81.8	69.4	0.3	19.6	**67.0**	**4.5**	8.6	1.9	0.2	0.1	0.1	17.4
	(mm)	neg	-8.0	-17.5	-19.3	-14.5	-12.5	-10.8	-13.2	0.3	3.9	**-13.7**	**-50.3**	19.6	0.4	-33.0	-44.2	-78.5	-45.3
	Z-axis	pos	0.1	0.3	0.3	0.1	0.2	0.1	0.2	0.5	0.1	**0.2**	**0.9**	0.3	0.4	0.7	0.7	1.4	0.8
	(mm)	neg	-66.4	-54.6	-46.5	-103.0	-74.5	-66.8	-57.6	0.3	18.3	**-67.1**	**-49.2**	12.3	0.3	-64.1	-42.6	-36.3	-54.0
L1	X-axis	pos	10.5	11.6	28.0	12.9	12.8	17.6	11.5	0.4	6.2	**15.0**	**15.7**	4.6	0.3	11.8	21.5	17.3	12.4
	(mm)	neg	-21.0	-5.8	-0.1	-17.1	-2.6	-7.4	-1.0	1.0	8.1	**-7.9**	**-3.7**	1.6	0.4	-3.3	-2.7	-2.8	-6.1
	Y-axis	pos	88.9	74.9	58.9	107.3	96.3	61.1	63.2	0.2	19.1	**78.7**	**3.3**	3.7	1.1	5.7	0.1	0.1	7.2
	(mm)	neg	-5.3	-10.3	-10.9	-11.3	-9.5	-6.4	-8.0	0.3	2.3	**-8.8**	**-51.0**	25.2	0.5	-40.6	-44.0	-87.9	-31.6
	Z-axis	pos	0.1	0.3	0.3	0.2	0.2	0.1	0.2	0.4	0.1	**0.2**	**1.6**	0.4	0.2	1.2	1.5	1.9	1.9
	(mm)	neg	-73.1	-66.5	-52.7	-103.5	-77.3	-90.4	-77.7	0.2	16.3	**-77.3**	**-66.2**	9.1	0.1	-73.3	-54.4	-63.9	-73.3
Sacrum	X-axis	pos	7.7	8.3	21.7	3.1	3.1	6.2	3.6	0.9	6.5	**7.7**	**6.8**	7.8	1.1	9.8	16.5	0.1	0.9
	(mm)	neg	-38.5	-5.9	-12.0	-60.0	-10.3	-21.6	-17.5	0.8	19.2	**-23.7**	**-15.7**	8.2	0.5	-18.4	-4.8	-15.1	-24.3
	Y-axis	pos	100.3	82.4	71.8	125.9	75.4	41.8	59.5	0.3	27.4	**79.6**	**2.6**	4.0	1.5	8.5	0.5	0.5	0.7
	(mm)	neg	-2.2	-1.8	-1.2	-3.6	-3.0	-2.0	-1.7	0.4	0.8	**-2.2**	**-41.8**	18.8	0.5	-36.1	-33.4	-69.5	-28.0
	Z-axis	pos	0.1	0.5	0.4	0.7	0.2	0.2	0.2	0.6	0.2	**0.3**	**1.6**	0.8	0.5	2.5	1.8	1.5	0.6
	(mm)	neg	-62.1	-43.5	-19.3	-84.8	-39.6	-42.8	-42.0	0.4	20.5	**-47.7**	**-37.4**	18.8	0.5	-61.6	-23.8	-42.9	-21.2
Unbelted Shoulder	X-axis	pos	100.0	69.8	76.1	63.2	63.9	117.5	99.3	0.3	21.3	**84.3**	**49.9**	2.1	0.0	51.5	47.6	51.7	48.6
	(mm)	neg	-69.7	-74.7	-88.5	-53.4	-56.0	-94.8	-82.8	0.2	15.7	**-74.3**	**-81.7**	23.8	0.3	-91.9	-110.4	-59.1	-65.4
	Y-axis	pos	171.0	278.1	346.5	179.2	158.6	250.3	236.9	0.3	67.7	**231.5**	**39.5**	43.9	1.1	50.3	10.8	0.1	96.8
	(mm)	neg	-59.2	-62.5	-69.1	-85.7	-84.3	-50.3	-48.3	0.2	15.0	**-65.6**	**-189.0**	49.8	0.3	-175.6	-244.8	-208.2	-127.4
	Z-axis	pos	7.8	5.8	5.8	35.1	25.9	27.1	25.4	0.6	12.1	**19.0**	**1.7**	0.8	0.5	1.1	2.9	1.4	1.4
	(mm)	neg	-171.4	-190.9	-209.4	-174.8	-147.6	-248.5	-224.6	0.2	34.6	**-195.3**	**-185.6**	20.1	0.1	-182.5	-214.3	-177.9	-167.8
Belted Shoulder	X-axis	pos	0.0	0.1	0.2	0.1	0.5	6.5	12.1	1.7	4.7	**2.8**	**8.8**	8.0	0.9	1.1	6.6	20.0	7.5
	(mm)	neg	-60.2	-116.9	-113.5	-54.0	-41.8	-58.9	-46.8	0.4	31.3	**-70.3**	**-63.1**	9.5	0.2	-76.8	-61.8	-54.8	-59.2
	Y-axis	pos	71.7	110.4	113.8	101.3	80.6	146.4	130.9	0.2	26.3	**107.9**	**54.7**	44.6	0.8	73.9	40.8	0.0	104.0
	(mm)	neg	-74.7	-82.4	-92.8	-96.0	-86.0	-68.2	-60.7	0.2	12.9	**-80.1**	**-100.7**	23.1	0.2	-91.1	-96.4	-134.1	-81.2
	Z-axis	pos	0.9	0.1	0.1	0.1	0.0	0.0	0.0	1.7	0.3	**0.2**	**46.3**	8.1	0.2	51.0	53.8	44.7	35.6
	(mm)	neg	-125.3	-141.1	-153.0	-152.3	-134.1	-108.2	-101.2	0.2	20.4	**-130.7**	**-101.5**	26.7	0.3	-113.9	-89.2	-71.2	-131.8

Table A2. Summary of Peak Values for PMHS Spine Segment Extensions and Rotations for Leading-Side and Trailing-Side Positions.

			Leading-Side										Trailing-Side						
			1890	**1897**	**1898**	**1905**	**1906**	**1913**	**1914**	**COV**	**SD**	**AVE**	**AVE**	**SD**	**COV**	**1894**	**1902**	**1910**	**1918**
Head to T1 Segment	Extension (mm)	pos	51.7	52.2	55.5	22.3	30.1	53.7	66.9	0.3	15.6	47.5	44.5	25.9	0.6	57.2	39.8	10.5	70.4
		neg	-0.2	0.0	-1.1	-13.9	-5.2	-3.4	-0.2	1.5	5.0	-3.4	-10.1	9.7	1.0	-9.2	-3.6	-24.0	-3.5
	X-axis Rotation (Degrees)	pos	13.0	19.1	24.3	10.9	6.6	19.2	11.1	0.4	6.2	14.9	17.8	3.8	0.2	16.2	22.8	18.4	13.9
		neg	-17.5	-0.3	-1.0	-4.1	-6.3	-9.6	-20.8	0.9	8.0	-8.5	-11.8	9.3	0.8	-21.3	-0.5	-8.2	-17.3
	Y-axis Rotation (Degrees)	pos	47.1	47.8	58.7	25.8	23.2	41.5	46.7	0.3	12.8	41.5	23.1	9.9	0.4	35.3	24.4	11.4	21.1
		neg	-36.2	-38.8	-39.2	-33.7	-32.1	-44.5	-38.4	0.1	4.1	-37.6	-43.8	14.8	0.3	-64.2	-37.7	-29.4	-43.9
T1 to T4 Segment	Extension (mm)	pos	6.4	3.4	6.2	4.2	3.9	3.4	4.6	0.3	1.3	4.6	6.2	1.9	0.3	7.0	3.8	5.7	8.3
		neg	-0.7	-1.9	-2.3	-4.6	-5.3	-7.4	-5.6	0.6	2.4	-4.0	-2.5	0.6	0.2	-3.3	-2.4	-2.1	-2.2
	X-axis Rotation (Degrees)	pos	16.3	21.5	26.0	15.9	11.2	20.5	18.2	0.3	4.7	18.5	20.5	6.3	0.3	20.9	28.6	13.4	19.2
		neg	-2.5	-0.1	-0.3	-1.1	-3.0	-3.3	-6.0	0.9	2.1	-2.3	-5.2	3.0	0.6	-3.0	-2.8	-5.4	-9.4
	Y-axis Rotation (Degrees)	pos	9.0	18.8	27.2	9.7	5.3	27.3	25.0	0.5	9.4	17.5	10.4	6.8	0.7	16.6	5.5	3.6	15.9
		neg	-13.2	-14.0	-14.5	-21.2	-18.7	-16.3	-14.8	0.2	2.9	-16.1	-20.7	2.8	0.1	-18.6	-24.5	-21.2	-18.4
T4 to T10 Segment	Extension (mm)	pos	0.1	6.1	8.1	0.1	8.9	11.6	14.7	0.8	5.5	7.1	11.9	12.2	1.0	5.5	3.2	29.8	9.0
		neg	-13.8	-2.8	-6.9	-18.5	-5.2	-6.1	-5.3	0.7	5.6	-8.4	-7.5	11.5	1.5	-24.5	-4.7	-0.5	-0.5
	X-axis Rotation (Degrees)	pos	9.3	14.5	19.2	9.7	10.0	16.0	13.2	0.3	3.7	13.1	14.4	4.0	0.3	9.8	19.4	13.2	15.1
		neg	-0.9	0.0	0.0	-0.4	0.0	-1.1	-2.3	1.2	0.8	-0.7	-3.0	1.2	0.4	-3.9	-1.7	-4.1	-2.1
	Y-axis Rotation (Degrees)	pos	3.2	14.2	19.7	11.3	9.4	31.3	28.8	0.6	10.3	16.8	13.2	8.1	0.6	9.6	7.5	10.4	25.2
		neg	-13.8	-11.9	-12.6	-16.4	-13.8	-11.3	-10.0	0.2	2.1	-12.8	-13.5	3.7	0.3	-11.8	-13.7	-18.5	-9.9
T10 to L1 Segment	Extension (mm)	pos	3.8	0.3	2.2	12.0	4.7	0.2	2.6	1.1	4.0	3.7	1.5	0.7	0.5	1.3	0.9	2.4	1.2
		neg	-7.3	-11.8	-6.7	-5.0	-4.6	-22.8	-18.1	0.7	7.1	-10.9	-21.3	9.3	0.4	-13.0	-14.8	-33.1	-24.4
	X-axis Rotation (Degrees)	pos	2.1	1.8	3.4	2.9	4.0	6.9	6.7	0.5	2.1	4.0	6.4	3.1	0.5	5.7	5.2	3.8	10.9
		neg	-14.9	-11.2	-6.2	-16.5	-5.4	-4.6	-4.7	0.6	5.1	-9.1	-9.0	10.0	1.1	-4.2	-4.3	-23.9	-3.5
	Y-axis Rotation (Degrees)	pos	0.0	0.0	0.0	0.1	0.3	11.5	6.8	1.7	4.6	2.7	6.4	4.2	0.7	5.1	2.6	12.4	5.5
		neg	-15.4	-24.1	-14.4	-27.0	-18.7	-8.1	-8.3	0.4	7.3	-16.5	-5.7	1.0	0.2	-4.8	-5.3	-7.1	-5.8
L1 to Sacrum Segment	Extension (mm)	pos	9.1	25.8	37.3	18.6	36.3	46.3	30.6	0.4	12.5	29.1	25.6	15.6	0.6	8.1	30.0	19.5	44.7
		neg	-7.3	-3.6	-2.1	-21.6	-3.2	-0.1	-0.4	1.4	7.5	-5.5	-2.7	3.1	1.1	-7.4	-0.6	-1.2	-1.7
	X-axis Rotation (Degrees)	pos	1.4	0.3	0.0	0.0	0.0	0.0	0.0	1.8	0.5	0.3	1.8	2.1	1.1	4.9	1.3	0.5	0.6
		neg	-15.0	-3.3	-7.6	-17.0	-7.2	-8.8	-8.4	0.5	4.8	-9.6	-11.2	2.6	0.2	-14.6	-8.5	-10.3	-11.5
	Y-axis Rotation (Degrees)	pos	0.8	0.0	0.2	0.0	5.8	5.6	4.1	1.1	2.7	2.4	5.7	0.7	0.1	5.2	5.4	6.7	5.4
		neg	-7.1	-6.5	-6.0	-7.3	-6.3	-1.5	-2.0	0.5	2.4	-5.2	-4.3	1.3	0.3	-4.3	-4.2	-6.0	-2.8